Journal of the Mechanical Behavior of Biomedical Materials 178 (2026) 107411

Contents lists available at ScienceDirect

Journal of the Mechanical Behavior of Biomedical Materials

journal homepage: www.elsevier.com/locate/jmbbm

Low-cost Ti alloys: assessment of their microstructure, mechanical properties, corrosion behaviour, and biological response

L. Bolzoni [a,*], W. Nishio [b], A.M. Appadan [b], B. Manogar [a]

[a] School of Engineering, The University of Waikato, Hamilton, 3240, New Zealand
[b] School of Dentistry, Cardiff University, Cardiff, CF14 4XY, UK

ARTICLE INFO

Keywords:
Implants
Titanium alloys
Wettability
Cytotoxicity
Selective attachment

ABSTRACT

Orthopaedic and dental implants, the majority of which are made from titanium alloys, face the crucial challenge of both inducing osteogenesis whilst inhibiting bacterial biofilm formation in an economical manner over the life of the implant. This study introduces an innovative strategy combining cost-effective alloying elements, selected due to their reported biological benefits, for developing new titanium alloys that achieve a tailorable mechanical, corrosion, and biological response. The combination of alloying and manufacturing results in homogeneous materials characterised by a lamellar microstructure. The developed low-cost Ti alloys have a maximum ultimate compression strength of 659 MPa, maximum tensile yield stress of 606 MPa, and maximum elongation of 8.3% without failing catastrophically. The alloys do not degrade as abiotic corrosion is significantly hampered by their intrinsic passivation behaviour (maximum corrosion rate of 8.9 μm/year), and have adjustable surface wettability with contact angles in the 60-81° range. Consequently, stomal cell attachment, cytotoxicity and cytokine production (IL-6 and TGF-β1), and antibacterial rate on *S. aureus* are consistent and comparable to those of current implnat materials. Based on these characteristics, the low-cost Ti alloys are promising materials for load-bearing biomedical devices.

1. Introduction

Amongst metallic biomaterials for load-bearing implants, titanium (Ti) alloys are preferred over alternatives such as stainless steel and CoCr alloys due to their lightweight properties; high mechanical strength capable of sustaining loads associated with physical activities (Geetha et al., 2009; Bolzoni et al., 2020); stiffness more compatible with that of human bone; corrosion resistance in a wide range of aggressive environments; and biocompatibility (Niinomi, 2008; Bolzoni et al., 2011). Ti is the preferred material for dental and orthopaedic implants, being extensively used for orthodontic devices, plates and screws for bone fixation, surgical instruments and artificial joint components (Geetha et al., 2009; Szczęsny et al., 2022; Oliveira et al., 2002). Despite extraordinary advances, commercial Ti alloys for biomedical applications are still characterised by long-lasting limitations related to potentially toxic elements (e.g. Al (Perl, 1985) and V (Domingo, 2002)), an inability to deter bacterial biofilm formation (Mahmoudi et al., 2022), and high production costs (Jia et al., 2018; Sjafrizal et al., 2020). The former two can be addressed by designing new Ti alloy compositions using appropriate elements and the latter by using alternative manufacturing techniques such as powder metallurgy (Sun et al., 2024; Raynova et al., 2019). It is worth mentioning that coatings (e.g., Ag) can be applied to Ti-based implants however they are characterised by significant limitations, such as a short antimicrobial lifespan (days to weeks), contribution towards antimicrobial resistance, and susceptibility to delamination and release of debris.

When considering the selection of alloying elements to design new compositions with tailored biomedical performance, the addition of Cu has primarily been investigated to achieve antibacterial properties (Ohkubo et al., 2003; Zhu et al., 2000; Kikuchi et al., 2003a; Zhang et al., 2016a, 2016b, 2016c; Yi et al., 2020; Wang et al., 2019; Liu et al., 2014; Alqattan et al., 2020); the addition of Fe has been used to reduce the intrinsic cost of the alloy and improve mechanical properties (Chen et al., 2011; Bolzoni, 2019; Niu et al., 2021; Romero et al., 2020, 2021; Chen and Hwang, 2012; Raynova et al., 2021); the addition of Nb mainly targeted the reduction of stiffness (Han et al., 2015; Lee et al., 2002; Xu et al., 2009; Manogar et al., 2022; Kikuchi et al., 2003b; Zhao et al., 2013; Yılmaz et al., 2018; Kalita et al., 2020); and the addition of Mn was analysed as a potential candidate to replace V due to its lower toxicity (Alqattan et al., 2020; Gouda et al., 2016; Cho et al., 2014;

* Corresponding author.
E-mail address: bolzoni.leandro@gmail.com (L. Bolzoni).

https://doi.org/10.1016/j.jmbbm.2026.107411
Received 28 January 2026; Received in revised form 26 February 2026; Accepted 10 March 2026
Available online 11 March 2026

Fernandes Santos et al., 2016; Kim et al., 2016). It is worth mentioning that the majority of the previously cited studies were carried out in binary systems (e.g. Ti-Cu alloys) aiming at improving a single specific property (e.g. antibacterial resistance via Cu addition). A survey of the current literature indicates that research where two of the previously mentioned alloying elements (i.e., Cu + Fe, Fe + Nb, Mn + Fe, and Mn + Nb) were synergistically amalgamated to concurrently improve competitive properties are scarce, and they have severe limitations. For instance, the few reports on ternary Ti-xFe-yCu alloys (Cho et al., 2013; Zadorozhnyy et al., 2012, 2017; Chaussê de Freitas et al., 2020) available did not quantify the antibacterial response, whilst the biological response of ternary Ti-xNb-yFe alloys (Hsu et al., 2010; Ehtemam-Haghighi et al., 2016a, 2016b, 2016c; Afonso et al., 2017; Li et al., 2019; Salvador et al., 2017; Chirico et al., 2020) is still undetermined in the literature. The same applies to ternary Ti-xNb-yMn alloys where the only two studies available (Chen et al., 2017; Ehtemam-Haghighi et al., 2019) exclusively focused on the mechanical behaviour. Similarly, ternary Ti-xFe-yMn alloys were studied by Ikeda et al. (2012) who focused their efforts in clarifying the phase constitution after heat treatments using electrical resistivity, Vickers hardness, and X-ray diffraction (XRD).

The alloying elements previously mentioned (i.e., Cu, Fe, Nb, and Mn) are either essential elements for the human body or are claimed to be non-toxic. Specifically, metabolic processes are supported by Cu (Zhang et al., 2019), where a lack of Cu (as well Mn) intake is detrimental for the proliferation, differentiation and migration of osteoblast cells, and for bone induction (Strause et al., 1987). Furthermore, it has been proven that angiogenesis is promoted both *in vitro* and *in vivo* (Wu et al., 2012) and skin defect healing is enhanced by Cu^{2+} ions (Wu et al., 2013). It is well established that the insufficient intake of Fe leads to anaemia as the human body is not capable of producing enough haemoglobin (Aspuru et al., 2011). The effect of Nb on the human body has not been extensively studied and has no known biological use, but Nb has been reported to be a non-toxic element (Liu et al., 2023). In the case of Mn, this element is needed to promote enzymes and amino acid metabolism, and to support the proper development of bone and skeletal growth (Miao and Clair, 2009).

We previously reported the development of ternary Ti alloys considering the combined lean additions of isomorphous and eutectoid beta stabilisers (Bolzoni et al., 2022) proving the feasibility of the proposed manufacturing approach, and demonstrating that materials with homogeneous distribution of the alloying elements are achieved. In the current study we therefore focused on the characterisation of their biological response with the aim of filling the current gap in the literature and providing a new strategy for achieving sound structural and biological performance. The study is complemented by the analysis of the mechanical and corrosion behaviour of the new low-cost Ti alloys developed by the joint addition of Cu, Fe, Nb, and Mn in pairs. It is worth noting that the amount of each alloying element was fixed at 2 wt percentage (i.e., wt.%) in an effort to develop α+β Ti alloys, which are those characterised by the best compromise between strength and toughness as required by structural biomedical implants. The novelty resides in the use of alloying elements rather than the ones (i.e., Al and V) used in commercial Ti prostheses with the aim of promoting an autogenous antibacterial response while controlling the cytotoxicity so that the alloy can promote osteointegration while simultaneously preventing short and long term bacterial infections, which is not the case of existing commercial biomedical titanium alloys.

2. Experimental procedure

2.1. Specimen preparation

The chosen Ti alloy compositions (i.e., Ti-2Cu-2Fe, Ti-2Fe-2Nb, Ti-2Mn-2Nb, and Ti-2Mn-2Fe) were obtained using the classical powder metallurgy route entailing cold pressing and vacuum sintering. For that, commercially available powders with suitable characteristics were purchased and include: Ti from GoodFellow (D_{90} < 75 μm, purity >99.4%, irregular), Cu from Merck KGaA (D_{90} < 63 μm, purity >99.7%, dendritic), Fe from GoodFellow (D_{90} < 10 μm, purity >99.0%, spherical), Nb from AlfaAesar (D_{90} < 45 μm, purity >99.8%, irregular), and Mn from Sigma-Aldrich (D_{90} < 45 μm, purity >99.0%, angular). Powder blends were obtained via mixing (30 min, 45 rpm) and were subsequently cold uniaxially pressed at 600 MPa and sintered at 1300 °C for 2 h in order to obtain a 40 mm diameter specimen per composition.

2.2. Microstructural analysis

XRD analysis (30-80° diffraction angle, 0.013°/s step size, CuK_{α}, Philips X'pert), density quantification through water displacement measurements (entailing measurements of the mass in air and water), and optical microscopy (Olympus BX53) were used to analyse the microstructure. For the latter, samples were metallographically prepared and chemically etched using a Kroll reactant (2 vol% HF + 4 vol% HNO_3 in distilled water) for 10 s prior to their microstructural characterisation.

2.3. Mechanical properties

Cylindrical samples, at least three per composition, with an approximate height (9 mm) to diameter (6 mm) ratio of 1.5 were used to quantify the compression behaviour (ASTM E9) of the alloys (viz., 0.54 mm/min strain rate) using an Instron 5982 universal tester. A minimum of five Vickers (HV) hardness measurements were performed to quantify the hardness of the alloys. The tensile behaviour (ASTM E8) of the low-cost Ti alloys was quantified using dogbone specimens with rectangular cross-section (viz., 2 x 2 mm^2 with 20 mm gauge length) tested at a strain rate of 1 mm/min using an Instron 33R4204 testing machine. A minimum of three dogbone specimens per composition were tested. Fractographic analysis was performed on the fracture surface of the tensile specimens by means of a scanning electron microscope Hitachi S4700.

2.4. Corrosion behaviour

Electrochemical properties of the low-cost Ti alloys were measured using a standard three-electrode configuration system in an eDAQ e-corder 410 electrochemical potentiostat. The samples served as the working electrode, a Pt wire was used as the counter electrode, and a standard Ag/AgCl was used as the reference electrode. The electrochemical measurements were performed at room temperature (i.e., 25 ± 1 °C) using as electrolyte a standard Hanks' balanced salt solution (i.e., simulated body fluid, SBF with pH 7.4) with composition of 8 g/l NaCl, 1 g/l glucose, 0.35 g/l $NaHCO_3$, 0.4 g/l KCl, 0.14 g/l $CaCl_2$, 0.1 g/l $MgCl_2{\cdot}6H_2O$, 0.06 g/l KH_2PO_4, 0.06 g/l $NaH_2PO_4{\cdot}2H_2O$, and 0.06 g/l $MgSO_4{\cdot}7H_2O$. After 1 h of stabilisation time to reach a steady potential (ISO 10271:2001), the potentiodynamic polarisation curves were acquired at a scanning rate of 50 mV/s from −2 V to 0 V. The corrosion potential E_{corr} (V) and the corrosion current density i_{corr} (nA/cm^2) were determined from the respective Tafel curves along with the anodic (β_a) and cathodic (β_c) Tafel slopes (V/dec). The driving force for passivation, or Gibbs free energy (ΔG), was quantified as $\Delta G = -n{\cdot}F{\cdot}E_{corr}$ (kJ/mol), where n is the number of electrons exchanged in the reaction and F is the Faraday constant (96,485 C/mol). The corrosion rate (CR, μm/year) was calculated as $CR = (0.00327{\cdot}M{\cdot}i_{corr})/(n{\cdot}d)$ where M is the molar mass of Ti (g/mol) and d the density of the material.

2.5. Water contact angle

Cylindrical samples, 10 mm in diameter and 2 mm in height, were manufactured as previously outlined for biological testing along with similar sized wrought Ti6Al4V discs purchased from Goodfellow (Cambridge, UK). To normalise sample surfaces for water contact angle,

cell and bacterial attachment studies, all samples were polished with silicon carbide paper to an average roughness (R_a) of 0.20 ± 0.05 μm and average maximum peak to valley distance (R_y) of 2.0 ± 0.5 μm. Roughness measurements were performed using a Surftest SV-2000 surface profilometer with Surfpak-SV software version 1.3 (Mitutoyu, Kanagawa, Japan) at a speed of 0.5 mm/s and 800 μm range across 8 mm of the sample surface. To assess the effect of alloy composition on the hydrophobicity of the surfaces, which is an important parameter for mediating mammalian and bacterial cell attachment (Webb et al., 1998; Oh et al., 2018), samples were cleaned with 70 vol% ethanol and air dried before a 4 μL drop of water was dispensed on the surface and the contact angle measured using a Theta Lite Optical Tensiometer with OneAttension software (Biolin, Stockholm, Sweden). Three samples per group were measured at room temperature to obtain average water contact angle values for each alloy.

2.6. Cytotoxicity

To determine the biocompatibility of the low-cost Ti alloys, a cell counting kit 8 assay (CCK-8) was performed. Sample discs were sterilised in an autoclave and heated to 121 °C for 15 min before cooling and being used for cytotoxicity and bacterial tests. Human bone marrow stromal cells (hBMSCs) were purchased and characterised by Lonza (Slough, UK) and used between passage numbers 4 to 8. hBMSCs were cultured in α-MEM medium supplemented with 10 vol% foetal bovine serum, 100 units/mL penicillin G sodium, 0.1 μg/mL streptomycin sulphate and 0.25 μg/mL amphotericin solution until 80% confluent, with media changed every 2-3 days. Cells were then detached using Accutase cell detachment solution. 10,000 cells were subsequently seeded onto each disc sample in 12 well plates and allowed to attach for 1 h at 37 °C, 5% CO_2. Wells were flooded with 1 mL of complete culture medium, and samples incubated for 24, 48 or 72 h. At each timepoint, the media was removed and the cells washed with 1 mL of sterile phosphate buffered saline (PBS) before incubation with 1 mL of complete media containing 100 μL of CCK-8 assay reagent. Samples were incubated at 37 °C, 5% CO_2 for 3 h before the supernatant was transferred to a 96-well plate and the absorbance measured at 450 nm with a wavelength correction of 650 nm. Ti-6Al-4V was selected as the control for biological testing as it is considered the gold standard Ti alloy for biomedical implants. Percentage viability relative to Ti-6Al-4V was calculated using equation (1):

$$Percentage\ viability = \frac{Sample\ absorbance\ at\ 450\ nm}{Average\ Ti-6Al-4V\ absorbance\ at\ 450nm} \times 100 \quad \text{Eq. 1}$$

2.7. Cell morphology

To further assess the impact of alloy composition on cell behaviour, cell morphology was assessed using phalloidin staining to visualise the actin cytoskeleton of hBSMCs on the surface of samples. Following 72 h incubation on the surface of the discs, hBMSCs were washed with 1 mL of PBS and fixed in 10% formalin for 10 min at room temperature. Samples were washed three times in PBS before permeabilising the cells with 1% Triton X-100 in PBS for 5 min at room temperature. Samples were subsequently washed with PBS three times and incubated in 1% bovine serum albumin in PBS for 30 min at room temperature to block non-specific binding sites. Cells were then incubated with 1 unit of phallotoxin using phalloidin conjugated with fluorescein isothiocyanate (phalloidin-FITC, Sigma-Aldrich, UK) for 30 min in the dark at room temperature. Samples were washed three times in PBS and allowed to dry in the dark before adding 10 μL of 1 mg/mL 4',6-diamidino-2-phenylindole (DAPI, Thermofisher, UK) to each sample surface to stain the nuclei of the cells. Cells were imaged using an AX70 Olympus Provis fluorescent microscope.

2.8. TGF-β1 and IL-6 production

To assess the regenerative and inflammatory cell response to the low-cost Ti alloys, 10,000 hBMSCs were seeded on the sterile sample surfaces in 12-well plates and allowed to attach for 1 h at 37 °C, 5% CO_2. Wells were flooded with complete culture medium, and samples incubated for 24, 48 or 72 h in 1 mL of media. At each timepoint, the media was removed and stored at −20 °C. Samples were thawed and analysed using human TGF-β1 and IL-6 ELISA kits (DuoSet ELISA kits, R&D Systems, Abingdon, UK) according to the manufacturer's instructions.

2.9. Bacterial attachment

To determine the antibacterial and anti-adherent properties of the low-cost Ti alloys, gram-positive *Staphylococcus aureus* NCTC 7791 (isolated from a human case of osteomyelitis) was incubated on the surface of the samples and colony forming unit (CFU) counts as well as live/dead staining was performed. Single colonies of *S. aureus* NCTC 7791 were isolated from tryptone soya agar streak plates and cultured in 20 mL of tryptone soya broth at 37 °C, 5% CO_2 overnight. The suspension was centrifuged at 3000 rpm for 5 min and the pellet was resuspended in 20 mL sterile PBS. The pellet was centrifuged again at 3000 rpm for 5 min and resuspended in PBS to achieve an absorbance of 0.08-0.1 at 600 nm corresponding to approximately 1×10^7 CFU/mL. To determine bacterial attachment, sterile discs were placed in 24-well plates and 1 mL of the 1×10^7 CFU/mL bacterial suspension in PBS was added onto the surface of the discs. After 1 h incubation at 37 °C, 5% CO_2, the discs were transferred onto a sterile 24-well plate and gently washed with 1 mL solution of 0.85% NaCl to remove non-adherent bacteria. 1 μL of syto9 and 1 μL of propidium iodide were added to 1 mL of 0.85% NaCl solution (LIVE/DEAD® BacLight™ Bacterial Viability stain, Life Technologies, Paisley, UK) and 20 μL of this solution added to the surface of the discs, covered with a sterile glass coverslip and left at room temperature for 5 min. Five random images of the disc surface were taken using an AX70 Olympus Provis fluorescent microscope at x10 magnification at emission/excitation wavelengths of 485/530-630 nm respectively.

Bacterial coverage was quantified using a macro written in ImageJ that calculates the percentage of the image occupied by fluorescence (Ayre et al., 2015). To establish bacterial viability the experiment was repeated, however at each time point following incubation with the bacteria, the samples were transferred onto a sterile 24-well plate and gently washed with 1 mL solution of 0.85% NaCl to remove non-adherent bacteria. The samples were then vortex-mixed in 1 mL of PBS in a universal container for 30 s to remove bacteria adherent to the alloy surface. The suspensions were serially diluted and spiral plated on tryptone soya agar using a Don Whitley Automated Spiral Plater fitted with a Don Whitley 602 Vacuum Pump (Don Whitley Scientific, UK). Agar plates were incubated for 24 h at 37 °C, 5% CO_2 before counting colonies.

2.10. Statistical analysis

The results of the physical and mechanical properties as well as corrosion behaviour were statistically analysed by a *t*-test (GraphPad Prism 10.4.1) and were considered statistically significant at $^{*}p < 0.05$ and $^{\#}p < 0.01$. Similarly, for all biological studies (cytotoxicity, cell morphology, TGF-β1 and IL-6 production and bacterial attachment), data from three independent experiments were collected. Statistical analysis was performed using the same software. Data was initially assessed for normality using a Shapiro-Wilk test. The water contact angle data was considered non-parametric and therefore a Kruskal-Wallis test with Dunn's post-hoc multiple comparisons was performed. Cytotoxicity, TGF-β1 and IL-6 production and bacterial attachment data was found to be parametric and therefore statistical significance was determined by a one-way ANOVA followed by Tukey's post hoc

multiple-comparison test. P-values ≤0.05 were considered as statistically significant. Data in the figures were presented as means ± standard deviation.

3. Results

3.1. Microstructural analysis

The results of the microstructural characterisation of the low-cost Ti alloys, which include XRD, relative density, and micrographs, are shown in Fig. 1, where it can be seen that exclusively the α-Ti phase was found in the XRD pattern of the Ti-2Cu-2Fe alloy. The α-Ti phase has a hexagonal closed packed structure whose lattice parameters are 2.95 Å and 4.67 Å for a and c, respectively. For all the other alloys, the α-Ti phase was found and was still the predominant phase, however peaks of the body centred cubic β-Ti phases (viz., a = 3.30 Å) were also detected. The relative intensity of the peaks of the β-Ti phase changes with the type of alloying elements used due to their different β-Ti phase stabilisation power. This is generally taken into account by means of the molybdenum equivalent parameter (Bania, 1994).

From Fig. 1b, which shows the variation of the relative density of the low-cost Ti alloys, it can be seen that a fairy comparable value (viz., 93.6-94.8%) was achieved regardless of the actual chemical composition. Consequently, the low-cost Ti alloys are characterised by the presence of residual porosity (5.2-6.4%) left by the sintering process (Wang et al., 2010) with an average pore size of 36 ± 12 μm. The minor variations in terms of relative density and associated porosity, which are statistically significant ($p < 0.05$), are mainly due to the alloying elements used and how much they promote the densification of the sample during sintering. The relative density values shown in Fig. 1b are, however, typical of Ti alloys obtained by means of powder metallurgy (Chen et al., 2011; Zhao et al., 2013; Fernandes Santos et al., 2016; Ehtemam-Haghighi et al., 2019) unless a pressure-assisted sintering technique is used to enhance the densification and reduce the overall amount of porosity (Bolzoni et al., 2012a, 2012b).

The analysis of the microstructure of the low-cost Ti alloys yields that they are characterised by the typical lamellar microstructure regardless of their actual chemistry. This type of microstructure is composed of α-Ti grains within which α-Ti + β-Ti lamellae are found, and is formed upon slow cooling from high temperatures in the β-Ti phase field. Nevertheless, it can be noticed that the features of the lamellar microstructure are remarkably affected by the chemical composition as the Ti-2Cu-2Fe alloy is characterised by coarse elongated α-Ti grains (Fig. 1c) whilst the other alloys have equiaxed α-Ti grains. Furthermore, it can be seen that the fineness of the microstructural features, especially that of the α-Ti + β-Ti lamellae, changes with the composition where the combined addition of Mn and Fe results in the finest microstructure (Fig. 1f). From the optical micrographs of Fig. 1 it can also be seen that uniformly distributed pores are present in the microstructure in agreement with the relative density data. The majority of these pores are almost spherical in shape and primarily found at the grain boundaries, although a minority of irregular pores and pores found inside the grains are also present.

3.2. Mechanical properties

The results of the analysis of the compressive and hardness behaviour of the low-cost Ti alloys are shown in Fig. 2. From the representative compressive stress-strain curves, it can be seen that the alloys have different stiffness and compressive response. The alloys are quite ductile, with minimum strain values of 36.1 ± 1.9 for the Ti-2Fe-2Cu alloy (Fig. 2a) and do not fail catastrophically. The lowest ultimate compression strength (viz., UCS) was obtained in the Ti-2Fe-2Nb alloy (viz., 1603 ± 38 MPa) and there is a very strong correlation between the UCS and the compressive yield stress (viz., CYS). There are variations in terms of both CYS (Fig. 2b) and the hardness (Fig. 2c) as a consequence of the difference in microstructural features and associated strengthening mechanisms. Therefore, the Ti-2Fe-2Nb alloy is the weakest (viz., 656 ± 21 MPa) and least hard (viz., 180 ± 3 HV), whilst the Ti-2Mn-2Fe alloy is the strongest (viz., 659 ± 9 MPa) and hardest (viz., 215 ± 4 HV),

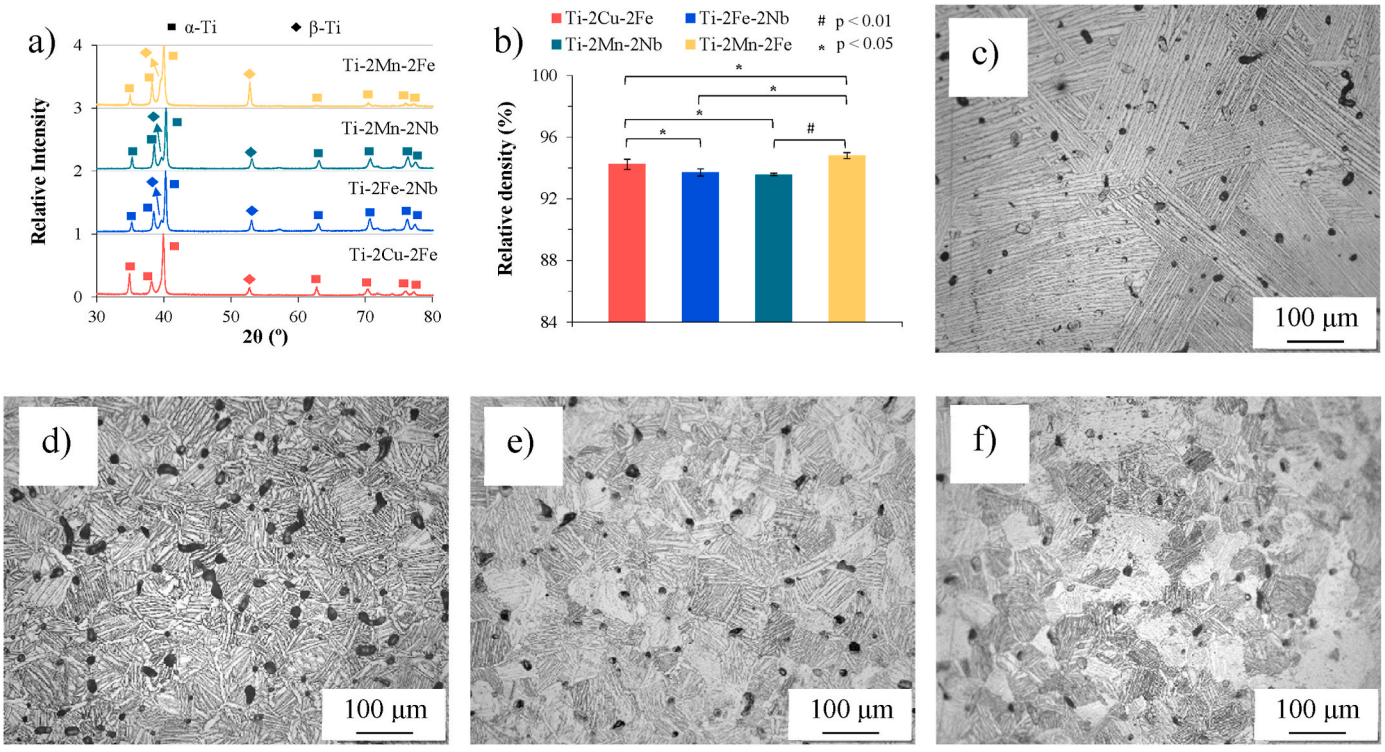

Fig. 1. Representative results of the microstructural characterisation of the low-cost Ti alloys: a) XRD patterns, b) relative density, and optical micrographs of the: c) Ti-2Cu-2Fe, d) Ti-2Fe-2Nb, e) Ti-2Mn-2Nb, and f) Ti-2Mn-2Fe alloys.

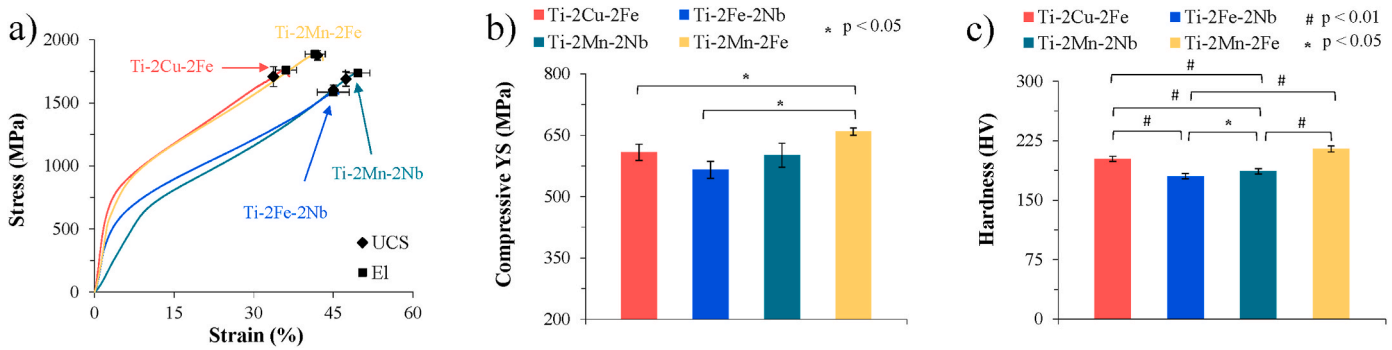

Fig. 2. Representative results of the mechanical properties of the low-cost Ti alloys: a) compression stress-strain curves, b) compressive yield stress, and c) hardness. Note: the values of the average ultimate compression strength (UCS) and strain (El) are shown along with the representative compression stress-strain curves.

which are statistically significant variations (at least $p < 0.05$).

The results of the analysis of the tensile and related fracture behaviour of the low-cost Ti alloys are shown in Fig. 3. The representative tensile curves show that the alloys had comparable Young modulus (viz., 95 ± 8 GPa) as the stress-strain curves overlapped in the elastic region. Independently of their actual chemical composition, the low-cost Ti alloys are able to undergo plastic deformation upon uniaxial tensile loading (Fig. 3a), however the actual load bearing capacity and amount of deformation prior to non-catastrophic failure is chemistry dependent ($p < 0.01$).

In agreement with the compression test results, the lowest and highest yield stress (YS) are found in the Ti-2Fe-2Nb (viz., 492 ± 8 MPa) and Ti-2Mn-2Fe (viz., 606 ± 6 MPa) alloy, respectively. Consistent with the tensile behaviour and the amount of plastic deformation the samples underwent, the fracture surfaces of the low-cost Ti alloys (Fig. 3c–f) are the results of ductile fracture due to a combination of transgranular and intergranular fracture of the α-Ti and β-Ti phases. The fracture surface is dominated by the presence of ductile dimples and a small amount of flat area with internal striations. The amount of dimples and flat areas are, respectively, significantly lower and higher in the Ti-2Mn-2Fe alloy in comparison to the other low-cost Ti alloys.

3.3. Corrosion behaviour

Fig. 4 shows the Tafel curves where it can be seen that the low-cost Ti alloys are characterised by a long passivation stage regardless of their actual composition. This indicates the formation of a stable protective passive layer, which is typical of Ti, and that the addition of the alloying elements does not disrupt the formation of such protective layer. Nevertheless, the actual composition of the low-cost Ti alloys affects the corrosion behaviour where Nb-containing alloys have more negative corrosion potentials (Fig. 4b) and anodic Tafel slope (Fig. 4c) values. The cathodic Tafel slope is fairly constant, with an average value of −0.23 ± 0.01 V/dec (Fig. 4d), and so is the passivation mean driving force (Figs. 4e), 254 ± 11 kJ/mol. The overall corrosion rate is comparable amongst the different low-cost Ti alloys and ranges from 6.8 μm/year for

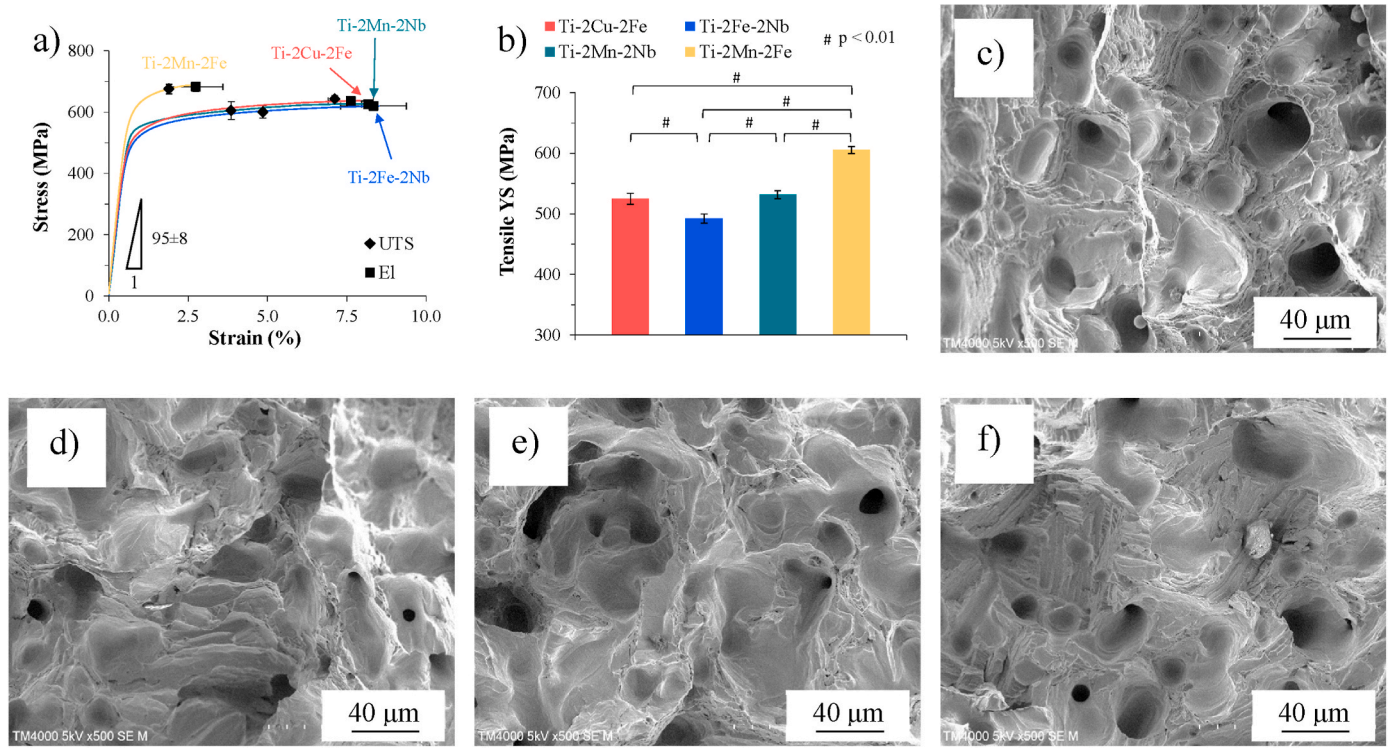

Fig. 3. Representative results of the tensile and fracture behaviour of the low-cost Ti alloys: a) tensile stress-strain curves, b) tensile yield stress, c) Ti-2Cu-2Fe, d) Ti-2Fe-2Nb, e) Ti-2Mn-2Nb, and f) Ti-2Mn-2Fe. Note: the values of the average ultimate tensile strength (UTS) and strain (El) are shown along with the representative tensile stress-strain curves.

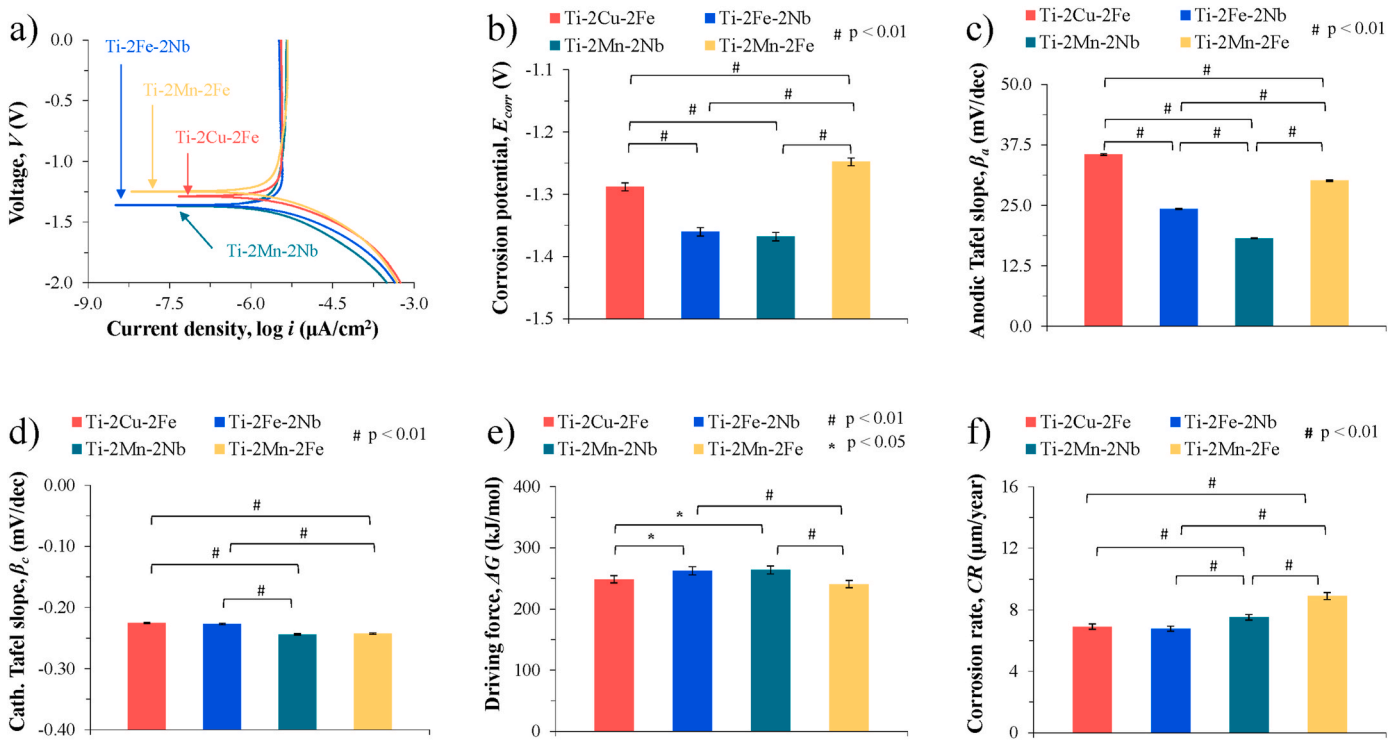

Fig. 4. Results of the characterisation of the corrosion behaviour of the low-cost Ti alloys: a) Tafel curves, b) corrosion potential (E_{corr}), c) anodic Tafel slope (β_a), d) cathodic Tafel slope (β_c), e) passivation driving force (ΔG), and f) corrosion rate (CR).

the Ti-2Fe-2Nb alloy to 8.9 μm/year for the Ti-2Mn-2Fe alloy (Fig. 4f), respectively. Most of the corrosion behaviour features analysed are statistically different ($p < 0.05$) amongst the different low-cost Ti alloys.

3.4. Water contact angle

The average water contact angles for the low-cost Ti alloys, along with that of the wrought Ti-6Al-4V alloy used as reference, are shown in Fig. 5. It was found that there were no significant differences between the wettability of medical grade Ti-6Al-4V and the low-cost Ti alloys ($p > 0.05$), with exception of Ti-2Mn-2Fe, where there is a slightly more pronounced reduction in water contact angle ($p < 0.05$), resulting in a more hydrophilic surface.

3.5. Biocompatibility and cell response

The cytotoxicity and cell response of the low-cost Ti alloys compared to Ti-6Al-4V are shown in Fig. 6 where it can be seen that there were no significant differences in raw absorbance values at 450 nm (Fig. 6a) and the percentage viability (Fig. 6b) of hBMSCs between all Ti-based alloys as determined by a CCK-8 assay ($p > 0.05$). Similarly, levels of the anti-inflammatory cytokine, TGF-β1 (Fig. 6c), and pro-inflammatory cytokine, IL-6 (Fig. 6d), across all Ti alloys are comparable, with no statistically significant differences between groups ($p > 0.05$); although the majority of the low-cost Ti alloys have slightly higher average values at the three incubation times analysed. The morphology of hBMSCs, as determined by actin cytoskeletal staining with phalloidin, are similar across all alloys (Fig. 6e–i), with spread spindle-shaped morphology indicating healthy attachment and no apoptosis or necrosis induced by the use of alternative alloying elements than the ones present in the commercial Ti-6Al-4V alloy used as a reference.

3.6. Bacterial attachment

The effect of the low-cost alloys on bacterial attachment is displayed

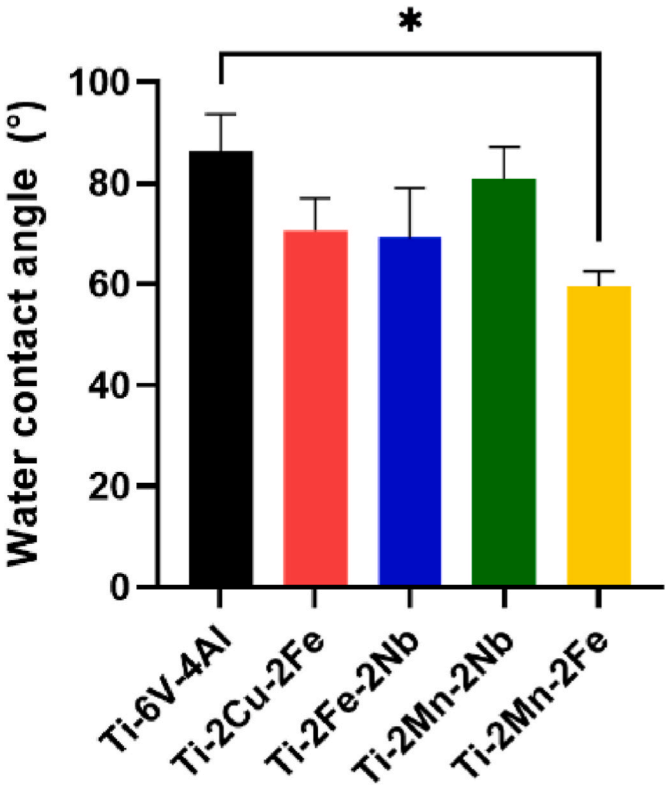

Fig. 5. Surface wettability of the low-cost Ti alloys as measured by water contact angle.

in Fig. 7 where it was found that gram-positive *S. aureus* NCTC 7791 (implicated in bone infections) readily attached to all alloy surfaces as per Fig. 7a–e, with limited cell death detected. When bacteria were

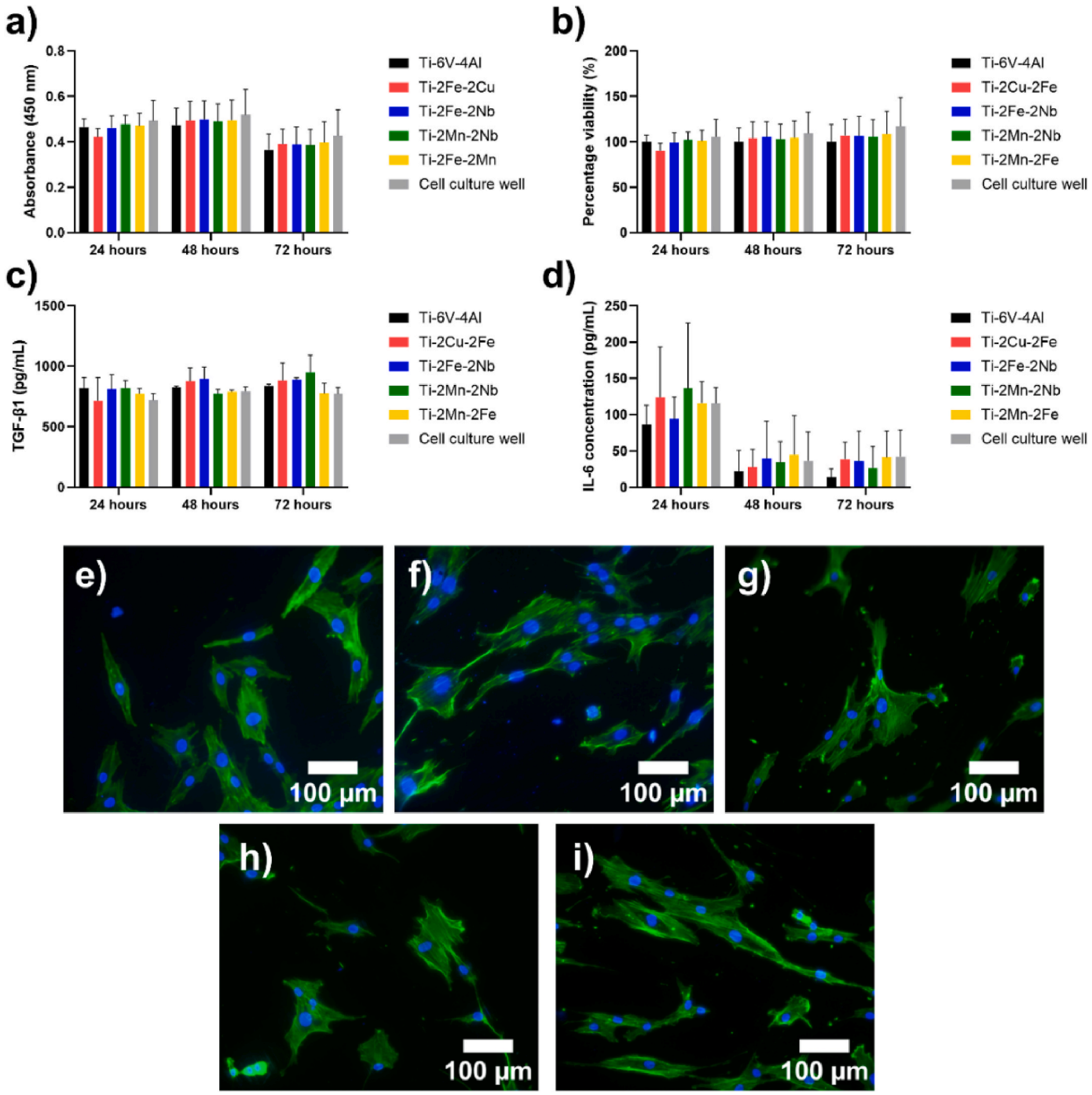

Fig. 6. Cytotoxicity and cell response of human bone marrow stromal cells on the surface of the low-cost Ti alloys: a) CCK-8 cytotoxicity results, b) percentage viability of cells relative to wrought Ti-6V-4Al, c) growth factor production (TGF-β1), d) inflammatory cytokine production (IL-6) and phalloidin staining of the actin cytoskeleton of hBMSCs, and representative images of the cell response on: e) Ti-6Al-4V, f) Ti-2Cu-2Fe, g) Ti-2Fe-2Nb, h) Ti-2Mn-2Nb, and i) Ti-2Mn-2Fe.

removed from the surface of the discs and colonies counted on agar plates, there were no statistically significant differences between the levels of attachment across all Ti-based alloys ($p > 0.05$). Similarly, when live/dead microscopy images were semi-quantified for percentage area covered with fluorescent bacteria, no significant differences between all alloy compositions ($p > 0.05$) were found. However, the distribution of the bacteria in the surface was affected by the actual microstructure as demonstrated by distinct attachment patterns.

4. Discussion

This study analysed the manufacturing and performance of ternary low-cost Ti alloys based on the addition of Cu, Fe, Nb, and Mn where two of these alloying elements were simultaneously added to create α+β Ti alloys, seeking the best compromise between strength and toughness in a cost-effective manner. Specifically, the Ti-2Cu-2Fe, Ti-2Fe-2Nb, Ti-2Mn-2Nb, and Ti-2Mn-2Fe alloys were obtained via powder metallurgy where each alloying elements was chosen because of their different biological footprints and ability to stabilise the β-Ti phase. This is commonly taken into account considering the molybdenum

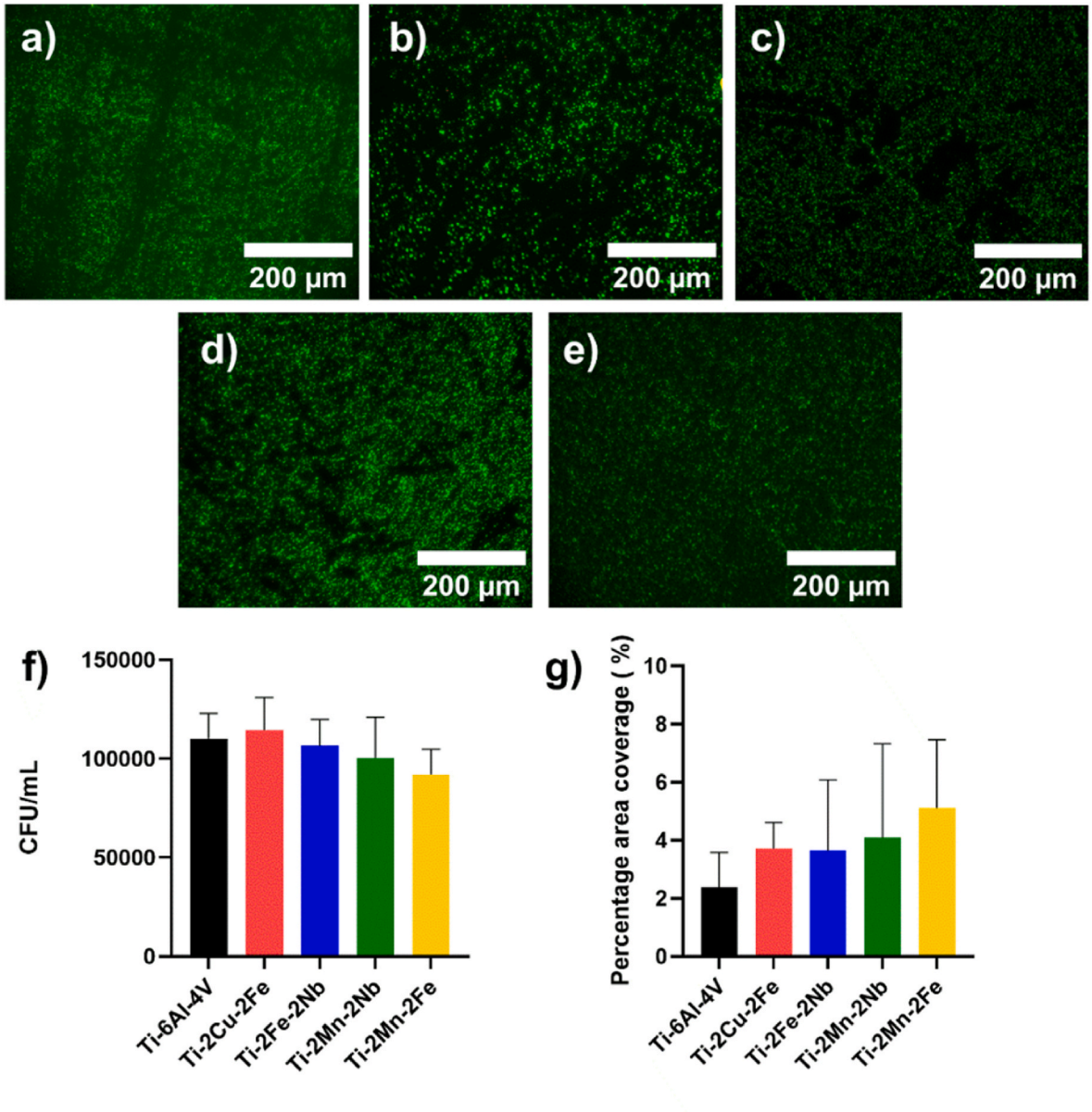

Fig. 7. Antibacterial properties the low-cost Ti alloys as assessed via live/dead staining of *Staphylococcus aureus* NCTC 7791 on the surface of: a) Ti-6Al-4V, b) Ti-2Cu-2Fe, c) Ti-2Fe-2Nb, d) Ti-2Mn-2Nb and e) Ti-2Mn-2Fe – live bacteria are stained green and dead bacteria are stained red; f) bacterial counts from the surface of the low-cost Ti alloys; and g) percentage area of the low-cost Ti alloys covered by bacteria. (For interpretation of the references to colour in this figure legend, the reader is referred to the Web version of this article.)

equivalent parameter and in this case the equation proposed by Bania (1994) was used (i.e., molybdenum equivalent = 0.28 Nb + 2.9 Fe + 0.77 Cu + 1.54 Mn, weighting factors for wt.% from quenched alloys). It was found that apart from the Ti-2Mn-2Nb alloy, all the low-cost Ti alloys had a molybdenum equivalent parameter between 5 and 10. Therefore, as per the classification proposed by Cotton et al. (2015), the low-cost Ti alloys are near-β alloys with the exception of the Ti-2Mn-2Nb alloy, which is considered a β-rich alloy. This is consistent with the result of the microstructural characterisation, which shows that all the low-cost Ti alloys are characterised by a lamellar microstructure.

The actual type and combination of alloying elements considered has, however, a remarkable effect on the microstructural features. Specifically, the microstructure of the Ti-2Cu-2Fe alloy is constituted by elongated α-Ti grains (i.e., prior β-Ti grains) and thick α-Ti and very thin β-Ti lamellae (Fig. 1c) as a consequence of the small amount of β-Ti phase stabilised. This was primarily due to the relatively small stabilising power of Cu as a eutectoid beta stabiliser and the fact that the amount of Fe added, which has a higher stabilising power, is not sufficient to form equiaxed α-Ti grains (Bolzoni et al., 2020). This is consistent with the XRD results shown in Fig. 1a) where only peaks of the α-Ti phase were found in the Ti-2Cu-2Fe alloy despite the clear presence of the β-Ti phase in the microstructure. As Cu was replaced by Nb in the Ti-2Fe-2Nb alloy, the microstructure changed to equiaxed due to the fact that Nb is an isomorphous beta stabiliser, meaning that Nb is soluble in both the α-Ti and β-Ti phases. Consequently, it can be seen that the overall size of the features of the lamellar microstructure is refined, resulting in the presence of α-Ti grains with smaller grain size and finer α-Ti + β-Ti lamellae as a consequence of the higher amount of β-Ti phase stabilised. Changing Fe for Mn (i.e., Ti-2Mn-2Nb), and using a combination of Fe + Mn, leads to the progressive refinement of the size of the α-Ti phase and the formation of subsequently finer α-Ti + β-Ti lamellae. Specifically, the thickness of the α-Ti lamellae decreases and that of the β-Ti lamellae increases, respectively, as dictated by the higher stabilisation power of the combinations of alloying elements used. This

trend is coherent with the evolution of the XRD patterns where the relative intensity of the diffraction peaks of the β-Ti phase increases, which is more relevant for the main peak of the β-Ti phase. The variation of the lamellar microstructure, which formed upon the slow cooling of the low-cost Ti alloys on crossing the allotropic phase transformation temperature, affects the mechanical properties, the corrosion behaviour, and the biological characteristics of the low-cost Ti alloys.

In agreement with the measurements of the relative density (Fig. 1b), the microstructural analysis shows that porosity is present in the microstructure of the low-cost Ti alloys. The residual pores are generally uniformly distributed throughout the microstructure, are primarily spherical in shape, and are found at the grain boundaries. These considerations indicate that the low-cost Ti alloys reached the last stage of sintering during the manufacturing where homogeneity of the chemical composition is expected (Chen et al., 2011; Zhao et al., 2013; Fernandes Santos et al., 2016; Ehtemam-Haghighi et al., 2019; Bolzoni et al., 2012c). This is reinforced by the fact that no undissolved powder particles of the alloying elements were found during the microstructural analysis. Although the variation of the relative density values of the different low-cost Ti alloys is low, it can be seen that the lowest value was obtained in the Ti-2Mn-2Nb alloy and the highest in the Ti-2Mn-2Fe alloy ($p < 0.01$), respectively. This is mainly related to the intrinsic physical properties of the alloying elements used. Specifically, Nb has a higher melting point with respect to the other elements and therefore has lower diffusivity, hindering the densification of the alloy. Additionally, Fe has higher diffusivity than Mn, despite the difference in melting point, and densification is also favoured by the smaller particle size of the Fe powder used to manufacture the low-cost Ti alloys.

Therefore, it is clear that the change in composition, as each low-cost Ti alloys is produced using different combinations of elemental powders, directly affects their manufacturability and the overall resultant behaviour in terms of structural properties, corrosion behaviour, water contact angle, and biological response. Fig. 8 shows the heatmap of the Spearman's rank correlation coefficient test used to clarify the relationship between composition-related aspects and the properties quantified. In terms of composition, it can be seen that there is a strong relationship between the amount of porosity and the molybdenum equivalent parameter as both are dependent on the specific alloying elements used. A slightly lower correlation is found with the relative intensity of the main β-Ti peak, which is an indication of the relative amount of β-Ti phase stabilised in the microstructure as compared to the α-Ti phase. Composition-related aspects have a remarkable influence on the structural properties (though much more explicit in the case of the tensile behaviour rather than compression as the former has more severe requirements in terms of material resistance), corrosion behaviour, water contact angle, and the cell/antibacterial response. Additionally, as a general trend, a longer incubation time results in better, or improved, correlations. This hints to the fact that short incubation times might not necessarily be the best option to quantify the actual long-term biological response of metallic biomaterials that occurs *in vivo*. As expected, structural properties have significant correlations amongst themselves; however, in the case of the low-cost Ti alloys a strong alloy also has good corrosion properties and biological response, which once again improves with the incubation time. A strong correlation is also found between the corrosion potential and the cytotoxic response at 72 h and the antibacterial rate as the intrinsic passivation behaviour of the low-cost Ti alloys influences the total amount of ions that can are released. The wettability, which include the wrought Ti-6Al-4V alloy as reference, is significantly more affected by the actual composition rather than the consequent amount of porosity, and in turns influences the biological behaviour, especially the pro-inflammatory cell response at long incubation times. Generally, fairly poor correlations are found between the different aspects of the biological response, even for the same trait (e.g., TGF-β1) but at different incubation times. Nevertheless, the low-cost Ti alloys show a progressively overall better biological response between cytotoxicity, pro-inflammatory cell, and antibacterial rate when longer incubation times are considered. From this whole overview analysed on the basis of the Spearman correlation heatmap, the most significant cases will further be discussed for an in-depth understanding of the effects of the different aspects on the comprehensive response of the low-cost Ti alloys.

The analysis of the mechanical behaviour of the low-cost Ti alloys demonstrates that failure did not occur catastrophically when either subjected to a uniaxial compressive load (Fig. 2a) or under an applied

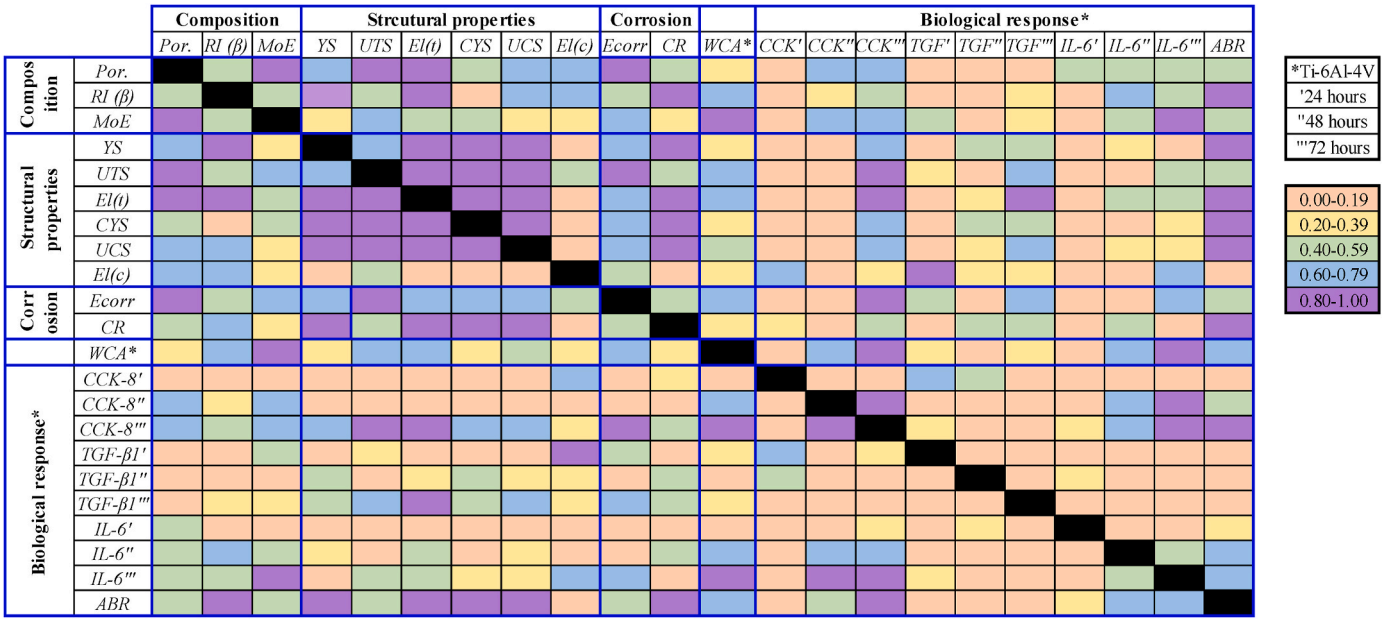

Fig. 8. Spearman correlation heatmap for the different properties of the low-cost Ti alloys. Legend: *Por.* – porosity; *RI (β)* – relative intensity of the main β-Ti peak; *MoE* – molybdenum equivalent parameter; *YS* – yield stress; *UTS* – ultimate tensile strength; *El(t)* – tensile strain; *CYS* – compressive yield stress; *CUS* – ultimate compressive strength; *El(t)* – compressive strain; E_{corr} – corrosion potential; *CR* – corrosion rate; *WCA* – water contact angle; *CCK* – CCK-8 cytotoxicity results (i.e., percentage viability of hBMSCs); *TGF* – TGF-β1 concentration (i.e., regenerative anti-inflammatory cytokine cell response); *IL-6* – IL-6 concentration (pro-inflammatory cytokine cell response); and *ABR* – antibacterial response.

uniaxial tensile force (Fig. 3a). This means that the low-cost Ti alloys are always able to undergo both elastic and plastic deformation upon mechanical loading. The actual composition did not affect the Young's modulus in tension but changed the stiffness in compression as well as the overall mechanical performance as indicated by compressive YS (Fig. 2b), tensile YS (Fig. 3b), and hardness (Fig. 2c) values. Representative variations of the mechanical behaviour of the low-cost Ti alloys are plotted in Fig. 9 as a function of the amount of porosity, the relative intensity of the main β-Ti peak, and as correlation between compression/tensile and hardness. Generally, a linear correlation between the mechanical properties and the selected parameters as well as amongst the different mechanical properties is found. In particular, a remarkably good correlation is found with the amount of porosity where the mechanical properties increase as the amount of residual pores present in the microstructure decreases (Fig. 9a, and Supplementary Fig. 1). This is the expected behaviour in alloys produced via powder metallurgy as residual pores act as stress concentration sites and, therefore, their size, morphology, and distribution affect the overall mechanical performance. It is also observed that, for each mechanical property, the lowest correlation is always found for the molybdenum equivalent parameter (Fig. 8, and Supplementary Fig. 1). This is due to the fact that the latter takes into account the overall β stabilisation strength of the alloying elements used but does not consider the actual features of the microstructural components (i.e., grain size, interlamellar spacing, etc.). Thus, better correlations are found with the relative intensity of the main β-Ti peak (Fig. 9b). Finally, a very good agreement is found between the compression and tensile response of the low-cost Ti alloys and their hardness (Fig. 9c). This is due to all of these properties being directly related to the different strengthening mechanisms active during the deformation (i.e., solid solution, ratio of the constituting phases, grain refinement, and porosity) of the low-cost Ti alloys. It is worth noticing that the highest coefficient of determination is always found for the UCS and the lowest for the YS, respectively. The variation of the mechanical performance is coherent with the results of the fractographic analysis (Fig. 3c–f) as the failing mechanism of the low-cost Ti alloys is primarily the combination of the fracture of the boundaries of the α-Ti grains and the fracture of the interphase boundaries between the α-Ti and β-Ti lamellae. As the strength of the low-cost Ti alloys increases, the amount of ductile dimples decreases and that of flat area (i.e., intergranular lamellar fracture) increases due to the refinement of the feature of the lamellar microstructure. The mechanical behaviour shown and the actual properties achieved, which are comparable to those of currently used Ti implants, are sufficient to sustain mechanical loads associated with physical activities without the loss of functionality of the implant. Specifically, the tensile strength is lower than that of forged Ti-6Al-4V alloy (i.e., 827 MPa yield stress) or Ti-6Al-7Nb alloy (i.e., 800 MPa yield stress) but higher than that of Ti grade 4 (i.e., 480 MPa yield stress). The elongation is lower as compared to Ti-6Al-4V/Ti-6Al-7Nb (i.e., 10%) and Ti (i.e., 15%), and so is the hardness. These differences are imputable to both the composition of the alloys as well as manufacturing method. If needed for the specific type of biomedical device, the mechanical properties of the low-cost Ti alloys (especially the ductility) can be improved by forging or hot isostatic pressing them to seal the residual porosity.

The analysis of the corrosion behaviour of the low-cost Ti alloys revealed that the alloys are capable of forming a stable protective passivity layer (Fig. 4). This confirms that the addition of the selected alloying elements does not hinder the passivation behaviour of Ti. However, the specific combination of alloying elements changes the characteristics of the corrosion response. The incorporation of Nb as alloying element leads to more negative passivation potential values and, hence, to a lesser tendency to form metal ions and a lower corrosion susceptibility (Fig. 4b). This results in a slightly higher thermodynamic driving force for passivation in these alloys due to the direct proportionality between the corrosion potential and the driving force (Fig. 4e). It is thus found that the Nb-containing alloys have lower corrosion rates where the highest value is in actuality found in the Ti-2Mn-2Fe alloy (Fig. 4f). This is due to the compromise between the thermodynamic driving force and the activation energy required for corrosion to start, and therefore the kinetics of the electrochemical reaction. The slope of the Tafel curves (Fig. 4a) is proportional to the corrosion reaction rate, and it is connected to the activation energy. The steeper the slope, the higher the activation energy, meaning that a greater overpotential change is needed for the same current density increase, resulting in slower corrosion kinetics. In terms of the cathodic Tafel slope (Fig. 4d) it is found that it is practically constant, regardless of the composition of the low-cost Ti alloys, as it is related to the corroding environment (i.e., Hanks' balanced salt solution in this instance). The anodic Tafel slope is directly affected by the composition of low-cost Ti alloys with steeper slopes in alloys where Nb is not present (Fig. 4c). The range of values found indicates that the corrosion and passivation of the low-cost Ti alloys is an activated controlled reaction limited by the transfer of electrons, which is generally characterised by Tafel slope between 30 and 120 mV/dec.

A more in-depth analysis of the parameters of the corrosion behaviour of the low-cost Ti alloys indicates that the corrosion potential and corrosion rate are the two that best reflect the changes induced by the variations of composition and microstructures (Fig. 8). Specifically, from Fig. 10 it can be seen that the corrosion potential is significantly affected by both the amount of porosity present in the microstructure and the actual type of alloying elements used as taken into account by means of the molybdenum equivalent parameter (Supplementary Fig. 2). Pores are cavities where the corrosion media (i.e., SBF) can penetrate and stagnate, leading to localised changes of the corrosive environment due to the formation of a differential aeration cell as a consequence of oxygen depletion inside the pore. Consequently, each pore becomes a more anodic (negative) with respect to the surrounding microstructure, which remains more cathodic (positive), and, therefore, faster localised corrosion occurs within the pores, as in crevice corrosion (He et al., 2002). Each specific alloying element has an associated β-Ti

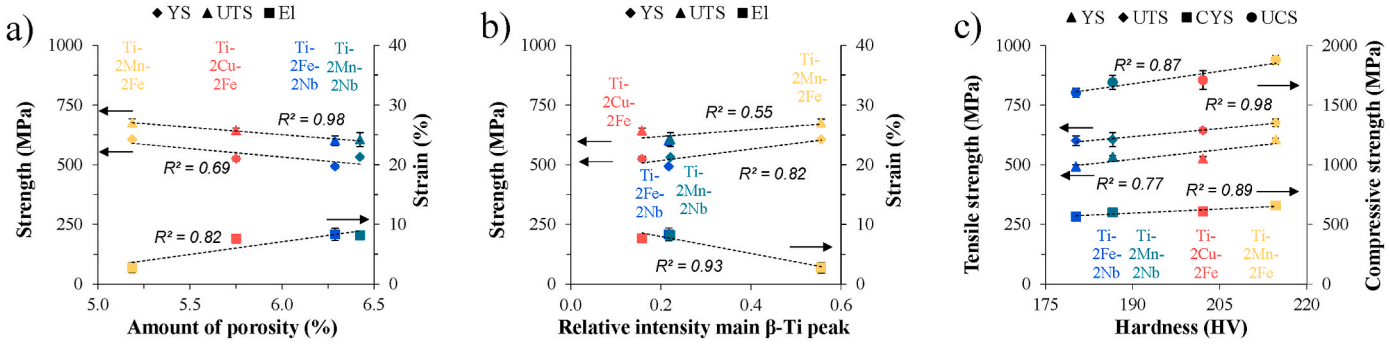

Fig. 9. Representative variations of the mechanical properties of the low-cost Ti alloys: a) tensile properties vs. amount of porosity, b) tensile properties vs. relative intensity of the main β-Ti peak, and c) tensile and compression strength vs. hardness.

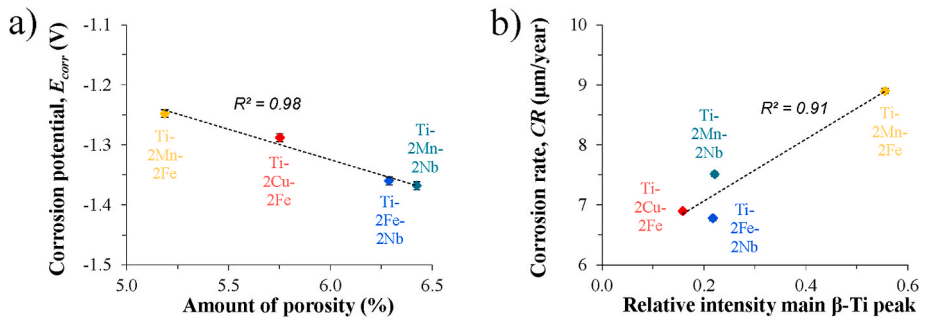

Fig. 10. Representative variations of the corrosion behaviour of the low-cost Ti alloys: a) corrosion potential (E_{corr}) vs. amount of porosity, and b) corrosion rate (CR) vs. relative intensity of the main β-Ti peak.

stabilisation power as well as a different solubility behaviour within the α-Ti and β-Ti phases. For instance, Nb is an isomorphous alloying elements soluble in both phases whereas Cu, Fe, and Mn are eutectoid alloying elements with progressively more limited solubility in the α-Ti phase. Consequently, this leads to the partitioning of the alloying elements within the α-Ti and β-Ti phases with the eutectoid alloying elements more heavily clustered in the β-Ti phase.

The difference in chemical composition between the α-Ti and β-Ti phases, the change in relative amount of these two phases as a consequence of using a more powerful beta stabiliser, and the local variations in chemistry between the phases due to partitioning of the alloying elements, all create very localised micro-galvanic cells. As the two metallic phases are in contact (i.e., electrically connected), the less noble of the α-Ti and β-Ti phases, which varies as a function of the chemistry, is more prone to undergo corrosion by releasing electrons when in contact with the electrolyte. This leads to the Ti-2Mn-2Fe alloy having the least negative corrosion potential, as Mn and Fe are the most active metals of the considered alloying elements, and the Nb-containing low-cost Ti alloys the more negative corrosion potentials. The corrosion rate is obviously affected by the corrosion potential, but it is much more so by the corrosion current density (i_{corr}), which takes into account the amount of electrical current flowing per unit area, as it is directly proportional to it. In this instance, the corrosion rate best fits with the relative intensity of the main β-Ti peak, which is an indication of the relative amount of β-Ti phase stabilised in the microstructure as compared to the α-Ti phase (Fig. 10b). The actual corrosion rate of the low-cost Ti alloys is, therefore, the compromise between the previously mentioned changes (e.g., relative amount of the α-Ti and β-Ti phases, partitioning) brought about from the use of different alloying elements and the intrinsic passivation behaviour of titanium. The latter leads to the formation of thin (i.e., few nm) superficial oxide layer, which is now directly interacting with the corrosive environment, resulting in the hindering of corrosion (Liu et al., 2023; Hacisalihoglu et al., 2015).

Amongst the low-cost Ti alloys, all samples have similar wettability characteristics with only the Ti-2Mn-2Fe alloy having a statistically significant ($p < 0.05$) lower water contact angle when compared to the industry standard for biomedical implants, Ti-6Al-4V (Fig. 5). The change in water contact angle is likely to be due to the differences in the features of the lamellar microstructure as the wrought Ti-6Al-4V alloy is also characterised by an α+β dual-phase microstructure containing numerous lamellar colonies (i.e., α-Ti grains) composed of alternating layers of α-Ti and retained β-Ti lamellae. The increasing of grain boundary density has been shown to increase water contact angle on nanocrystalline Au thin films (Ha et al., 2022) and, therefore, a refinement of the grain structure is expected to lead to a higher hydrophobicity; at least in single phase materials. In the case of the low-cost Ti alloys, the decrease of the contact angle is most likely due to the compositional changes and associated microstructure, which include amount of porosity and refinement of the lamellar microstructure due to the stabilisation of a greater amount of β-Ti phase (Fig. 1). When the water contact angle data are analysed against composition-related aspects, it can be seen from Fig. 11 that a strong correlation is found between the values of the water contact angle and the molybdenum equivalent parameter, which best reflect the stabilising power of the different alloying elements considered in the design of the low-cost Ti alloys. It is worth noticing that, in the case of the wrought Ti-6Al-4V, the value of the molybdenum equivalent parameter was calculated purely on the basis of V as Al is a alpha stabiliser element. Therefore, the hydrophilicity of the Ti alloy is controlled by the features of the lamellar microstructure rather than the presence of porosity, which has a poor correlation (Supplementary Fig. 3). Specifically, the addition of more powerful beta stabilisers increases the amount of retained β-Ti phase upon cooling and, consequently, increases the amount of interfaces between the α-Ti and β-Ti phases.

Across all the alloys tested, comparable cellular responses in terms of cytotoxicity and cytokine production (IL-6 and TGF-β1) were observed (Fig. 6). The actual low amount of each alloying element used (i.e., 2 wt %), which eventually results in low levels of ion released from the low-cost Ti alloys, yielded similar biological responses, even though the chosen alloying elements have been reported to have beneficial biological roles in bone repair. For instance, Mn, in the form of Mn^{2+} ions have been shown to be involved in integrin signalling, promoting osteoblast adhesion, viability and proliferation. A number of studies have demonstrated the beneficial effects of Mn in osteogenesis and bone repair (Taskozhina et al., 2024). Fe plays numerous roles in gene regulation, metabolism and hormone synthesis; however, its function is dose-dependent with Fe overload and deficiency being associated with bone weakening (Balogh et al., 2018). At appropriate doses, Fe ions

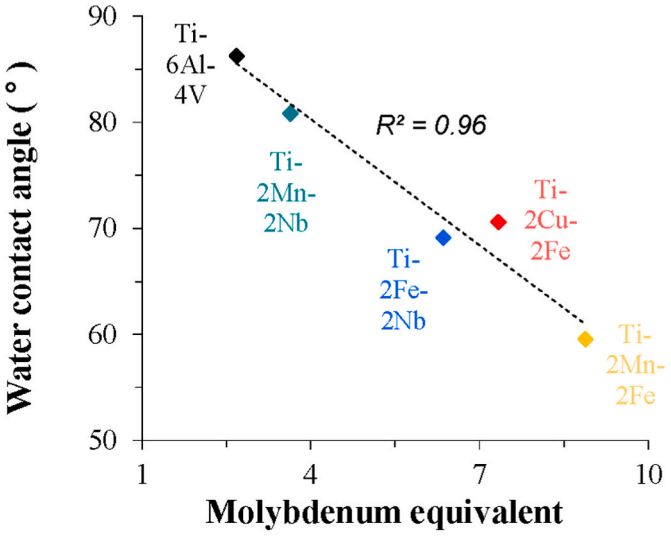

Fig. 11. Variation of the water contact angle of the low-cost Ti alloys vs. molybdenum equivalent parameter.

contribute to DNA synthesis, collagen production, and metabolism of vitamin D, critical processes for cell proliferation and bone matrix formation. Similarly, Cu is an essential trace element involved in enzymatic reactions, nucleic acid synthesis, antioxidant defence and immune function. Its predominant role in bone appears to be linked to vascularisation, with both deficiency and excess resulting in bone fragility (Zhang et al., 2024). Whilst Mn, Fe and Cu are all naturally found in the human body, Nb is not. As such, its biological function is less understood, however the metal is widely accepted to be biocompatible. When incorporated with gallium as nanofibre surfaces, Nb was shown to promote osteoblast differentiation and mineralisation through elevated expression of bone-related genes, such as alkaline phosphatase, osteocalcin, osteopontin and runt-related transcription factor 2; whilst also promoting M2 anti-inflammatory macrophage polarisation (Wei et al., 2023). The osteogenic effects of Nb have also been further validated in an *in vivo* rat fracture healing model (Tan et al., 2022). A comparison of the microstructure (Fig. 1) and cell response images (Fig. 6) shows that the hBMSCs easily attach to all of the low-cost Ti alloy surfaces without preferential sites, resulting in a homogenous distribution of cells with spread spindle-shaped morphology. The similar cellular responses found is, therefore, most likely a direct consequence of the passivation behaviour and short incubation time analysed (i.e., max 72 h) which seems not long enough to be able to explicitly capitalise on the desirable biological benefits derived by the addition of each specific alloying element.

The variation of the CCK-8 cytotoxicity results is plotted in Fig. 12 as a function of relevant affecting parameters, which include contact angle, amount of porosity, molybdenum equivalent parameter (Supplementary Fig. 4), and corrosion behaviour. It can be noticed that, regardless of the parameter considered, the response of the cells after 24 h of incubation always has an opposite trend to those of 48 and 72 h. Specifically, the percentage viability of hBMSCs increases with the contact angle for 24 h but decreases in the other two cases, and it decreases with the amount of porosity and molybdenum equivalent for 24 h, but it increases for 48 and 72 h of incubation. The only exception to this common behaviour is the variation of the cells percentage viability with the corrosion rate (*CR*), which is much more directly related to the formation of the protective passivation layer (Fig. 12b). Additionally, it is consistently found that much better correlations are found for 48 h and 72 h with respect to 24 h (once again with the exception of the corrosion behaviour) with the best correlations always found for the longest incubation time considered (Fig. 8). When considering the behaviour of anti-inflammatory cells, generally the response after 24 and 72 h of incubation has similar trends (e.g., increasing) with composition-related aspects, but the trend is the opposite for 48 h (Fig. 12c) with, once again, the exception of the corrosion rate (*CR*). Generally, the best coefficients of determination are found for the longest incubation time analysed as the TGF-β1 concentration is a specific aspect of the regenerative response (Fig. 8, and Supplementary Fig. 5). In the case of the pro-inflammatory cell response the trend is constant across the incubation time as it always decreases/increases depending on the aspect considered (Fig. 8, and Supplementary Fig. 6). For instance, it decreases against the contact angle (Fig. 12e), but it increases with the corrosion rate (*CR*). As for the other cytotoxicity aspects, the best relationships are obtained after 72 h incubation time. These overall trends reflect the time needed for the cells to adjust to specific surface, and its features (e.g., amount of stabilised β-Ti phase). On a comparative basis, it can also be seen that the Mn-bearing low-cost Ti alloys have a much more consistent average cytotoxicity response across the different incubation times whist higher variabilities are found for the Fe-bearing low-cost Ti alloys, especially when Cu is present. This is a consequence of the chemical activity and mobility of the atoms of the selected alloying elements as Nb is the most stable due to its higher melting point and Cu the smaller atomic radius.

From the literature, elements such as Cu are well known to induce antimicrobial activity (Salah et al., 2021), though across all alloys tested, the attachment and viability of *S. aureus*, a pathogen highly implicated in orthopaedic infections, was not notably reduced. This is due to the short incubation time used (i.e., 1 h of incubation time) which

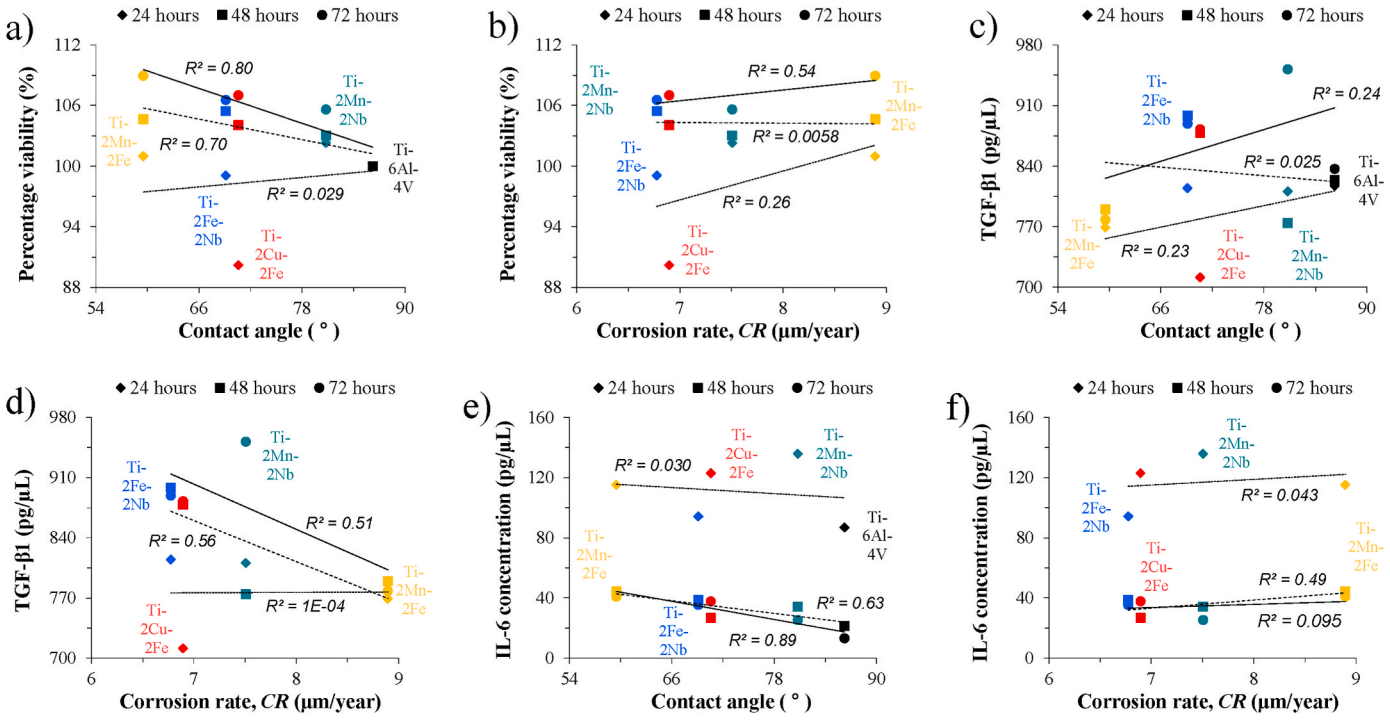

Fig. 12. Representative variations of the cytotoxicity results of the low-cost Ti alloys: a) percentage viability of hBMSCs (CCK-8) vs. water contact angle, b) percentage viability of hBMSCs (CCK-8) vs. corrosion rate (*CR*), c) regenerative anti-inflammatory cytokine cell response (TGF-β1 concentration) vs. water contact angle, d) regenerative anti-inflammatory cytokine cell response (TGF-β1 concentration) vs. corrosion rate (*CR*), e) pro-inflammatory cytokine cell response (IL-6 concentration) vs. water contact angle, and f) pro-inflammatory cytokine cell response (IL-6 concentration) vs. corrosion rate (*CR*).

seems not long enough to harvest the potential benefits where, for instance, in the literature, antibacterial capability after 24 h of incubation has been reported for solid Cu-bearing Ti alloys. Nonetheless, bacterial attachment was also not increased by the composition of the low-cost Ti alloys, which is important given that Fe plays a critical role in bacterial physiology and pathogenesis, particularly in biofilm formation (Oliveira et al., 2021). Mn has also been shown to play similar roles to Fe in bacterial pathogenesis, in particular, detoxifying reactive oxygen species and protecting against neutrophil killing (Juttukonda et al., 2017). Other studies however have shown different forms of Mn, for example MnO nanoparticles (Saod et al., 2022), display strong antibacterial activity. Despite the overall similar antibacterial attachment quantified as percentage area coverage, a direct comparison of the microstructure (Fig. 1) and live-dead staining images (Fig. 7) reveals an interesting finding. The surface of the wrought Ti-6Al-4V alloys is fully covered by a homogeneous dense layer of *S. aureus* as is the surface of the Ti-2Mn-2Fe alloy, which is characterised by a very lamellar microstructure. The features of the lamellar microstructure are coarser for the Ti-2Mn-2Nb and Ti-2Fe-2Nb alloys, respectively, and it can be seen that a more heterogenous and less dense of layer of *S. aureus* bacteria is present (Fig. 7c–d). Specifically, there are some areas with no bacteria attached, which seems to coincide with the equiaxed grains containing coarse α-Ti lamellae combined with fine β-Ti lamellae. This effect is even more pronounced in the Ti-2Cu-2Fe alloy, which has coarse elongated α-Ti grains and extremely fine β-Ti lamellae (Fig. 7b). As previously discussed, the formation of elongated/equiaxed α-Ti grains and the fineness of the lamellae is dictated by the alloying element chosen and by their solubility within the α-Ti and β-Ti phases. Consequently, this seems to hint to the fact that antibacterial capability can be finely tuned by tailoring the features of the lamellar microstructure in Ti alloys, which will have to be investigated through dedicated experiments for confirmation. However, the basic analysis of the effect of composition-related aspects on the antibacterial attachment shows that the latter always increases monotonically with the refinement of the features of the lamellar microstructure (Fig. 13), with the exception of the case of the contact angle where a more hydrophobic surface reduces the bacteria attachment (Supplementary Fig. 7). An overall finer lamellar microstructure is associated with a more homogenous distribution of the alloying elements at an atomic/micro level, resulting in more localised variations of the internal electronic structure and associated micro-potential differences, which seems to be more favourable for bacterial attachment. Such localised variations lead to the presence of a different number of micro-galvanic corrosion cells of different sizes affecting the corrosion behaviour and the release of electrons. Smaller micro-galvanic corrosion cells entail higher current density or, in turns, higher corrosion rates (Fig. 4f) resulting in a linear relationship between the antibacterial attachment and corrosion rate (CR) in the low-cost Ti alloys (Fig. 13b). As previously shown (Wang et al., 2017), micro-galvanic corrosion cells are activated by the bacteria coming into contact with the metallic surface leading to the transfer of electrons, which enter the bacteria itself changing the internal electron transport chain. This disruptive action leads to the generation of reactive oxygen species which provoke intracellular oxidation, membrane potential variation, and cellular contents release and the, eventual, death of the bacteria. In the case of the low-cost Ti alloys, despite the reactive oxygen species, no elicit antibacterial activity in comparison to Ti-6Al-4V is found; however, the cell compatibility is also not compromised (Fig. 6).

Concluding, despite the limitations of this initial study, the biological data demonstrates that low-cost Ti alloys have similar biocompatibility to the biomedical standard alloy, Ti-6Al-4V, and do not induce greater levels of early bacterial colonisation. Whilst these results are promising, further *in vivo* tests are required to fully confirm the findings. Additionally, it would be interesting to assess whether higher concentrations of alloying metals are needed to observe stronger biological responses. Studies on binary Ti alloys, such as Ti-Cu, have shown successful antimicrobial activity, however many of these studies employ greater weight percentages of Cu, in the region of 5-10% (Mahmoudi et al., 2022), which can also be detrimental and lead to cuproptosis (Xie et al., 2023). Whilst the addition of a third metal into the Ti alloy may influence antibacterial activity, the low weight percentage employed in this study (2 wt%) may perhaps result in more subtle cellular and bacterial responses and therefore longer-term osteogenic or bacterial quorum sensing/biofilm assays are required to better understand the biological effects of these ternary alloys.

Looking forward, though the proposed alloys are potential candidates for structural biomedical devices further mechanical and biological characterisation is needed. Specifically, dynamic properties such fatigue response and fracture toughness will have to be quantified in terms of mechanical behaviour. Additionally, eventual approval will be needed for clinical translation for which initial *in vivo* studies in animals and further long-term *in vivo* studies to validate the biocompatibility and, if it is case, identify potential risks associated with the selected alloying elements will be required for regulatory purposes. Additionally, once the additional characterisation is successful, aspects related to the scalability of the proposed manufacturing technique will have to be addressed, especially in terms of economic feasibility and implementation challenges.

5. Conclusions

In this study, new α+β low-cost Ti alloys, fabricated using an alternative manufacturing technique and developed through the careful selection of non-toxic alloying elements essential for the human body, were proven to be promising candidates to be used in biomedical applications due to their comprehensive mechanical, corrosion, and biological behaviour. Manufacturing of the alloys via powder metallurgy guarantees achieving homogenous materials with a lamellar microstructure. In terms of mechanical performance, the alloys have an ultimate compression strength in the 565-659 MPa range, tensile yield stress in the 492-606 MPa range, and hardness values in the 180-215 HV

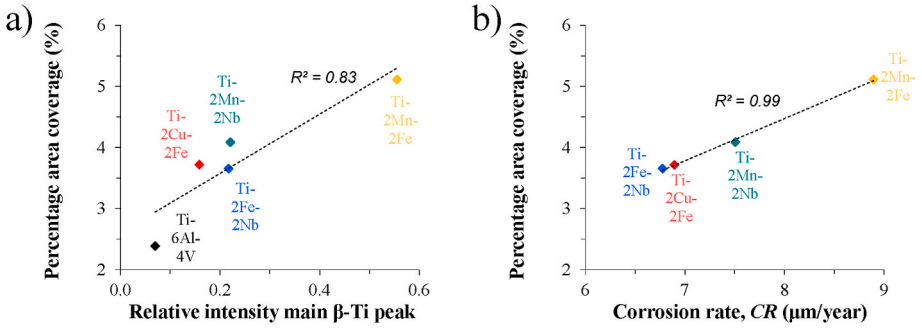

Fig. 13. Variation of the antibacterial response of the low-cost Ti alloys: a) bacterial attachment vs. relative intensity of the main β-Ti peak, and b) bacterial attachment vs. corrosion rate (*CR*).

range. The low-cost Ti alloys are able to withstand loads without failing catastrophically and their mechanical properties are higher than those of pure Ti used. The surface wettability of the low-cost Ti alloys is comparable to that of the Ti-6Al-4V used for biomedical implants, all of them below 90°. The cell attachment, cytotoxicity and cytokine production (IL-6 and TGF-β1), and antibacterial attachment rate against *S. aureus* of the low-cost Ti alloys is comparable to that of the Ti-6Al-4V alloy. Furthermore, this studies shows that biological benefits may be derived in the long-term which were not captured through the conducted short-term experiments.

CRediT authorship contribution statement

L. Bolzoni: Writing – review & editing, Methodology, Investigation, Conceptualization. **W. Nishio:** Writing – review & editing, Methodology, Investigation, Conceptualization. **A.M. Appadan:** Methodology, Investigation. **B. Manogar:** Methodology, Investigation.

Declaration of competing interest

The authors declare that they have no known competing financial interests or personal relationships that could have appeared to influence the work reported in this paper.

Acknowledgements

This work was supported by the Cardiff University and the University of Waikato Strategic International Partnership Collaborative Seed Fund. L.B. would like to thank Mr. Manpreet Paul for technical contributions.

Appendix A. Supplementary data

Supplementary data to this article can be found online at https://doi.org/10.1016/j.jmbbm.2026.107411.

Data availability

Data will be made available on request.

References

Afonso, C.R.M., Chaves, J.M., Florêncio, O., 2017. Effect of rapid solidification on microstructure and elastic modulus of β Ti-xNb-3Fe alloys for implant applications. Adv. Eng. Mater. 19 (6), 1600370.
Alqattan, M., Peters, L., Alshammari, Y., Yang, F., Bolzoni, L., 2020. Antibacterial ti-mn-cu alloys for biomedical applications. Regen. Biomater. 8 (1) rbaa050.
Aspuru, K., Villa, C., Bermejo, F., Herrero, P., López, S.G., 2011. Optimal management of iron deficiency anemia due to poor dietary intake. Int. J. Gen. Med. 4 (null), 741–750.
Ayre, W.N., Scott, T., Hallam, K., Blom, A.W., Denyer, S., Bone, H.K., Mansell, J.P., 2015. Fluorophosphonate-functionalised titanium via a pre-adsorbed alkane phosphonic acid: a novel dual action surface finish for bone regenerative applications. J. Mater. Sci. Mater. Med. 27 (2), 36.
Balogh, E., Paragh, G., Jeney, V., 2018. Influence of iron on bone homeostasis. Pharmaceuticals 11 (4), 107.
Bania, P.J., 1994. Beta titanium alloys and their role in the titanium industry. JOM 46 (7), 16–19.
Bolzoni, L., 2019. Low-cost Fe-bearing powder metallurgy Ti alloys. Met. Powder Rep. 74 (6), 308–313.
Bolzoni, L., Esteban, P.G., Ruiz-Navas, E.M., Gordo, E., 2011. Influence of powder characteristics on sintering behaviour and properties of PM Ti alloys produced from prealloyed powder and master alloy. Powder Metall. 54 (4), 543–550.
Bolzoni, L., Ruiz-Navas, E.M., Neubauer, E., Gordo, E., 2012a. Mechanical properties and microstructural evolution of vacuum hot-pressed titanium and Ti-6Al-7Nb alloy. J. Mech. Behav. Biomed. Mater. 9C, 91–99.
Bolzoni, L., Ruiz-Navas, E.M., Gordo, E., 2012b. Influence of vacuum hot-pressing temperature on the microstructure and mechanical properties of Ti-3Al-2.5V alloy obtained by blended elemental and master alloy addition powders. Mater. Chem. Phys. 137, 608–616.
Bolzoni, L., Esteban, P.G., Ruiz-Navas, E.M., Gordo, E., 2012c. Mechanical behaviour of pressed and sintered titanium alloys obtained from prealloyed and blended elemental powders. J. Mech. Behav. Biomed. Mater. 14, 29–38.
Bolzoni, L., Alqattan, M., Peters, L., Alshammari, Y., Yang, F., 2020. Ternary Ti alloys functionalised with antibacterial activity. Sci. Rep. 10 (1), 22201.
Bolzoni, L., Paul, M., Yang, F., 2022. Effect of combined lean additions of isomorphous and eutectoid beta stabilisers on the properties of titanium. J. Mater. Res. Technol. 21, 3828–3843.
Chaussê de Freitas, C., Campo, K.N., Caram, R., 2020. Thixoforming of titanium: the microstructure and processability of semisolid Ti-Cu-Fe alloys. Vacuum 180, 109567.
Chen, B.-Y., Hwang, K.-S., 2012. Sintered Ti-Fe alloys with in situ synthesized TiC dispersoids. Mater. Sci. Eng., A 541, 88–97.
Chen, B.-Y., Hwang, K.-S., Ng, K.-L., 2011. Effect of cooling process on the alpha phase formation and mechanical properties of sintered Ti-Fe alloys. Mater. Sci. Eng., A 528, 4556–4563.
Chen, Z., Liu, Y., Jiang, H., Liu, M., Wang, C.H., Cao, G.H., 2017. Microstructures and mechanical properties of Mn modified, Ti-Nb-based alloys. J. Alloys Compd. 723, 1091–1097.
Chirico, C., Tsipas, S.A., Wilczynski, P., Gordo, E., 2020. Beta titanium alloys produced from titanium hydride: effect of alloying elements on titanium hydride decomposition. Metals 10 (5), 682.
Cho, K., Niinomi, M., Nakai, M., Hieda, J., Kawasaki, Y., 2013. Development of high modulus Ti-Fe-Cu alloys for biomedical applications. Mater. Trans. 54 (4), 574–581.
Cho, K., Niinomi, M., Nakai, M., Hieda, J., Fernandes Santos, P., Itoh, Y., Ikeda, M., 2014. Mechanical properties, microstructures, and biocompatibility of low-cost β-Type Ti-Mn alloys for biomedical applications. Biomater. Sci.: Processing, Properties and Applications IV 251, 21–30.
Cotton, J.D., Briggs, R.D., Boyer, R.R., Tamirisakandala, S., Russo, P., Shchetnikov, N., Fanning, J.C., 2015. State of the art in beta titanium alloys for airframe applications. JOM 67 (6), 1281–1303.
Domingo, J.L., 2002. Vanadium and tungsten derivatives as antidiabetic agents: a review of their toxic effects. Biol. Trace Elem. Res. 88, 97–112.
Ehtemam-Haghighi, S., Liu, Y., Cao, G., Zhang, L.-C., 2016a. Phase transition, microstructural evolution and mechanical properties of Ti-Nb-Fe lloys induced by Fe addition. Mater. Des. 97, 279–286.
Ehtemam-Haghighi, S., Liu, Y., Cao, G., Zhang, L.-C., 2016b. Influence of Nb on the β→α″ martensitic phase transformation and properties of the newly designed Ti-Fe-Nb alloys. Mater. Sci. Eng. C 60, 503–510.
Ehtemam-Haghighi, S., Prashanth, K.G., Attar, H., Chaubey, A.K., Cao, G.H., Zhang, L.C., 2016c. Evaluation of mechanical and wear properties of TixNb7Fe alloys designed for biomedical applications. Mater. Des. 111, 592–599.
Ehtemam-Haghighi, S., Attar, H., Dargusch, M.S., Kent, D., 2019. Microstructure, phase composition and mechanical properties of new, low cost Ti-Mn-Nb alloys for biomedical applications. J. Alloys Compd. 787, 570–577.
Fernandes Santos, P., Niinomi, M., Liu, H., Cho, K., Nakai, M., Itoh, Y., Narushima, T., Ikeda, M., 2016. Fabrication of low-cost beta-type Ti-Mn alloys for biomedical applications by metal injection molding process and their mechanical properties. J. Mech. Behav. Biomed. Mater. 59, 497–507.
Geetha, M., Singh, A.K., Asokamani, R., Gogia, A.K., 2009. Ti based biomaterials, the ultimate choice for orthopaedic implants - a review. Prog. Mater. Sci. 54 (3), 397–425.
Gouda, M.K., Nakamura, K., Gepreel, M.A.H., 2016. Effect of Mn-Content on the deformation behavior of binary Ti-Mn alloys. Key Eng. Mater. 705, 214–218.
Ha, H., Ko, S., Goh, B., Müller, S., Baumann, R.-P., Leem, M., Jo Yoo, S., Choi, J., Hwang, B., 2022. Influence of grain boundary density on the surface energy of nanocrystalline metal thin films. Appl. Surf. Sci. 604, 154463.
Hacisalihoglu, I., Samancioglu, A., Yildiz, F., Purcek, G., Alsaran, A., 2015. Tribocorrosion properties of different type titanium alloys in simulated body fluid. Wear 332–333, 679–686.
Han, M.-K., Kim, J.-Y., Hwang, M.-J., Song, H.-J., Park, Y.-J., 2015. Effect of Nb on the microstructure, mechanical properties, corrosion behavior, and cytotoxicity of Ti-Nb alloys. Materials 8 (9), 5986–6003.
He, X., Noël, J.J., Shoesmith, D.W., 2002. Temperature dependence of crevice corrosion initiation on titanium Grade-2. J. Electrochem. Soc. 149 (9), B440.
Hsu, H.-C., Hsu, S.-K., Wu, S.-C., Lee, C.-J., Ho, W.-F., 2010. Structure and mechanical properties of As-cast Ti-5Nb-xFe alloys. Mater. Char. 61 (9), 851–858.
Ikeda, M., Ueda, M., Kinoshita, T., Ogawa, M., Niinomi, M., 2012. Influence of Fe content of ti-mn-fe alloys on phase constitution and heat treatment behavior. Mater. Sci. Forum 706–709, 1893–1898.
Jia, M.T., Gabbitas, B., Bolzoni, L., 2018. Evaluation of reactive induction sintering as a manufacturing route for blended elemental Ti-5Al-2.5Fe alloy. J. Mater. Process. Technol. 255, 611–620.
Juttukonda, L.J., Berends, E.T.M., Zackular, J.P., Moore, J.L., Stier, M.T., Zhang, Y., Schmitz, J.E., Beavers, W.N., Wijers, C.D., Gilston, B.A., Kehl-Fie, T.E., Atkinson, J., Washington, M.K., Peebles, R.S., Chazin, W.J., Torres, V.J., Caprioli, R.M., Skaar, E. P., 2017. Dietary manganese promotes staphylococcal infection of the heart. Cell Host Microbe 22 (4), 531–542.e8.
Kalita, D., Rogal, Ł., Czeppe, T., Wójcik, A., Kolano-Burian, A., Zackiewicz, P., Kania, B., Dutkiewicz, J., 2020. Microstructure and mechanical properties of Ti-Nb alloys prepared by mechanical alloying and spark plasma sintering. J. Mater. Eng. Perform. 29 (3), 1445–1452.
Kikuchi, M., Takada, Y., Kiyosue, S., Yoda, M., Woldu, M., Cai, Z., Okuno, O., Okabe, T., 2003a. Mechanical properties and microstructures of cast Ti-Cu alloys. Dent. Mater. 19 (3), 174–181.
Kikuchi, M., Takahashi, M., Okuno, O., 2003b. Mechanical properties and grindability of dental cast Ti-Nb alloys. Dent. Mater. J. 22 (3), 328–342.

Kim, J.-W., Hwang, M.-J., Han, M.-K., Kim, Y.-G., Song, H.-J., Park, Y.-J., 2016. Effect of manganese on the microstructure, mechanical properties and corrosion behavior of titanium alloys. Mater. Chem. Phys. 180, 341–348.
Lee, C.M., Ju, C.P., Chern Lin, J.H., 2002. Structure-property relationship of cast Ti-Nb alloys. J. Oral Rehabil. 29 (4), 314–322.
Li, Q., Miao, P., Li, J., He, M., Nakai, M., Niinomi, M., Chiba, A., Nakano, T., Liu, X., Zhou, K., Pan, D., 2019. Effect of Nb content on microstructures and mechanical properties of Ti-xNb-2Fe alloys. J. Mater. Eng. Perform. 28 (9), 5501–5508.
Liu, J., Li, F., Liu, C., Wang, H., Ren, B., Yang, K., Zhang, E., 2014. Effect of Cu content on the antibacterial activity of titanium-copper sintered alloys. Mater. Sci. Eng. C 35, 392–400.
Liu, H., Wang, Z.-X., Cheng, J., Li, N., Liang, S.-X., Zhang, L., Shang, F., Oleksandr, D., Chen, L.-Y., 2023. Nb-content-dependent passivation behavior of Ti-Nb alloys for biomedical applications. J. Mater. Res. Technol. 27, 7882–7894.
Mahmoudi, P., Akbarpour, M.R., Lakeh, H.B., Jing, F., Hadidi, M.R., Akhavan, B., 2022. Antibacterial Ti-Cu implants: a critical review on mechanisms of action. Mater. Today Bio 17, 100447.
Manogar, B., Yang, F., Bolzoni, L., 2022. Correlation between microstructure and tensile properties of powder metallurgy Ti-6Nb-x(Fe or mn) alloys. J. Alloys Compd. 926, 166805.
Miao, L., Clair, D.K. St, 2009. Regulation of superoxide dismutase genes: implications in disease. Free Radic. Biol. Med. 47 (4), 344–356.
Niinomi, M., 2008. Mechanical biocompatibilities of titanium alloys for biomedical applications. J. Mech. Behav. Biomed. Mater. 1 (1), 30–42.
Niu, J., Guo, Y., Li, K., Liu, W., Dan, Z., Sun, Z., Chang, H., Zhou, L., 2021. Improved mechanical, bio-corrosion properties and in vitro cell responses of Ti-Fe alloys as candidate dental implants. Mater. Sci. Eng. C 122, 111917.
Oh, J.K., Yegin, Y., Yang, F., Zhang, M., Li, J., Huang, S., Verkhoturov, S.V., Schweikert, E.A., Perez-Lewis, K., Scholar, E.A., Taylor, T.M., Castillo, A., Cisneros-Zevallos, L., Min, Y., Akbulut, M., 2018. The influence of surface chemistry on the kinetics and thermodynamics of bacterial adhesion. Sci. Rep. 8 (1), 17247.
Ohkubo, C., Shimura, I., Aoki, T., Hanatani, S., Hosoi, T., Hattori, M., Oda, Y., Okabe, T., 2003. Wear resistance of experimental Ti-Cu alloys. Biomaterials 24, 3377–3381.
Oliveira, M.V., Pereira, L.C., Cairo, C.A.A., 2002. Porous Structure Characterization in Titanium Coating for Surgical Implants. scielo, pp. 269–273.
Oliveira, F., Rohde, H., Vilanova, M., Cerca, N., 2021. The emerging role of iron acquisition in biofilm-associated infections. Trends Microbiol. 29 (9), 772–775.
Perl, D.P., 1985. Relationship of aluminum to Alzheimer's disease. Environ. Health Perspect. 149–153.
Raynova, S., Collas, Y., Yang, F., Bolzoni, L., 2019. Advancement in the pressureless sintering of CP titanium using high-frequency induction heating. Metall. Mater. Trans. 50 (10), 4732–4742.
Raynova, S., Yang, F., Bolzoni, L., 2021. The effect of thermomechanical treatments on the properties of powder metallurgy Ti-5Fe alloy. Mater. Sci. Eng., A 801, 140389.
Romero, C., Yang, F., Wei, S., Bolzoni, L., 2020. Thermomechanical processing of cost-affordable powder metallurgy Ti-5Fe alloys from the blended elemental approach: microstructure, tensile deformation behavior, and failure. Metals 10 (11), 1–16.
Romero, C., Yang, F., Raynova, S., Bolzoni, L., 2021. Thermomechanically processed powder metallurgy Ti-5Fe alloy: effect of microstructure, texture, Fe partitioning and residual porosity on tensile and fatigue behaviour. Materialia 20, 101254.
Salah, I., Parkin, I.P., Allan, E., 2021. Copper as an antimicrobial agent: recent advances. RSC Adv. 11 (30), 18179–18186.
Salvador, C.A.F., Dal Bó, M.R., Costa, F.H., Taipina, M.O., Lopes, E.S.N., Caram, R., 2017. Solute lean ti-nb-fe alloys: an exploratory study. J. Mech. Behav. Biomed. Mater. 65, 761–769.
Saod, W.M., Hamid, L.L., Alaallah, N.J., Ramizy, A., 2022. Biosynthesis and antibacterial activity of manganese oxide nanoparticles prepared by green tea extract. Biotechnol. Rep. 34, e00729.
Sjafrizal, T., Dehghan-Manshadi, A., Kent, D., Yan, M., Dargusch, M.S., 2020. Effect of Fe addition on properties of Ti-6Al-xFe manufactured by blended elemental process. J. Mech. Behav. Biomed. Mater. 102, 103518.
Strause, L., Saltman, P., Glowacki, J., 1987. The effect of deficiencies of manganese and copper on osteoinduction and on resorption of bone particles in rats. Calcif. Tissue Int. 41 (3), 145–150.
Sun, J., Pan, Y., Liu, Y., Kuang, F., Wu, X., Cao, P., Lu, X., 2024. The designed high-performance PM Ti-6Al-4V alloy via two-step pressureless sintering. J. Alloys Compd. 976, 173324.
Szczęsny, G., Kopec, M., Politis, D.J., Kowalewski, Z.L., Łazarski, A., Szolc, T., 2022. A review on biomaterials for orthopaedic surgery and traumatology: from past to present. Materials 15 (10), 3622.
Tan, J., Li, J., Cao, B., Wu, J., Luo, D., Ran, Z., Deng, L., Li, X., Jiang, W., Xie, K., Wang, L., Hao, Y., 2022. Niobium promotes fracture healing in rats by regulating the PI3K-Akt signalling pathway: an in vivo and in vitro study. J. Orthop. Transl. 37, 113–125.
Taskozhina, G., Batyrova, G., Umarova, G., Issanguzhina, Z., Kereyeva, N., 2024. The manganese-bone connection: investigating the role of manganese in bone health. J. Clin. Med. 13 (16), 4679.
Wang, H., Fang, Z.Z., Sun, P., 2010. A critical review of mechanical properties of powder metallurgy titanium. Int. J. Powder Metall. 46 (5), 45–57.
Wang, G., Jin, W., Qasim, A.M., Gao, A., Peng, X., Li, W., Feng, H., Chu, P.K., 2017. Antibacterial effects of ttitanium embedded with silver nanoparticles based on electron-transfer-induced reactive oxygen species. Biomaterials 124, 25–34.
Wang, J., Zhang, S., Sun, Z., Wang, H., Ren, L., Yang, K., 2019. Optimization of mechanical property, antibacterial property and corrosion resistance of Ti-Cu alloy for dental implant. J. Mater. Sci. Technol. 35 (10), 2336–2344.
Webb, K., Hlady, V., Tresco, P.A., 1998. Relative importance of surface wettability and charged functional groups on NIH 3T3 fibroblast attachment, spreading, and cytoskeletal organization. J. Biomed. Mater. Res. 41 (3), 422–430.
Wei, W., Yang, R., Yu, Q., Zhao, J., Li, W., 2023. Gallium-niobium nanofiber surface of Niobium/PEKK composite with anti-inflammatory, osteogenesis and anti-bacterial effects for facilitating osteoblastic differentiation and ameliorating osteointegration. Compos. B Eng. 248, 110375.
Wu, C., Zhou, Y., Fan, W., Han, P., Chang, J., Yuen, J., Zhang, M., Xiao, Y., 2012. Hypoxia-mimicking mesoporous bioactive glass scaffolds with controllable cobalt ion release for bone tissue engineering. Biomaterials 33 (7), 2076–2085.
Wu, C., Zhou, Y., Xu, M., Han, P., Chen, L., Chang, J., Xiao, Y., 2013. Copper-containing mesoporous bioactive glass scaffolds with multifunctional properties of angiogenesis capacity, osteostimulation and antibacterial activity. Biomaterials 34 (2), 422–433.
Xie, W., Guo, Z., Zhao, L., Wei, Y., 2023. The copper age in cancer treatment: from copper metabolism to cuproptosis. Prog. Mater. Sci. 138, 101145.
Xu, L.-J., Xiao, S.-l., Tian, J., Chen, Y.-y., Huang, Y.-d., 2009. Microstructure and dry wear properties of Ti-Nb alloys for dental prostheses. Trans. Nonferrous Met. Soc. China 19, s639–s644.
Yi, C.B., Ke, Z.Y., Zhang, L., Tan, J., Jiang, Y.H., He, Z.Y., 2020. Antibacterial Ti-Cu alloy with enhanced mechanical properties as implant applications. Mater. Res. Express 7 (10), 105404.
Yılmaz, E., Gökçe, A., Findik, F., Gulsoy, H.O., 2018. Metallurgical properties and biomimetic HA deposition performance of Ti-Nb PIM alloys. J. Alloys Compd. 746, 301–313.
Zadorozhnyy, V.Y., Inoue, A., Louzguine-Luzgin, D.V., 2012. Ti-based nanostructured low-alloy with high strength and ductility. Mater. Sci. Eng., A 551, 82–86.
Zadorozhnyy, V.Y., Shi, X., Kozak, D.S., Wada, T., Wang, J.Q., Kato, H., Louzguine-Luzgin, D.V., 2017. Electrochemical behavior and biocompatibility of ti-fe-cu alloy with high strength and ductility. J. Alloys Compd. 707, 291–297.
Zhang, E., Ren, J., Li, S., Yang, L., Qin, G., 2016a. Optimization of mechanical properties, biocorrosion properties and antibacterial properties of As-cast Ti-Cu alloys. Biomed. Mater. 11 (6), 065001.
Zhang, E., Wang, X., Chen, M., Hou, B., 2016b. Effect of the existing form of Cu element on the mechanical properties, bio-corrosion and antibacterial properties of Ti-Cu alloys for biomedical application. Mater. Sci. Eng. C 69, 1210–1221.
Zhang, E., Li, S., Ren, J., Zhang, L., Han, Y., 2016c. Effect of extrusion processing on the microstructure, mechanical properties, biocorrosion properties and antibacterial properties of Ti-Cu sintered alloys. Mater. Sci. Eng. C 69, 760–768.
Zhang, E.-L., Fu, S., Wang, R.-X., Li, H.-X., Liu, Y., Ma, Z.-Q., Liu, G.-K., Zhu, C.-S., Qin, G.-W., Chen, D.-F., 2019. Role of Cu element in biomedical metal alloy design. Rare Met. 38 (6), 476–494.
Zhang, Z., Tang, H., Du, T., Yang, D., 2024. The impact of copper on bone metabolism. J. Orthop. Transl. 47, 125–131.
Zhao, D., Chang, K., Ebel, T., Qian, M., Willumeit, R., Yan, M., Pyczak, F., 2013. Microstructure and mechanical behavior of metal injection molded Ti-Nb binary alloys as biomedical material. J. Mech. Behav. Biomed. Mater. 28, 171–182.
Zhu, K.Y., Zhao, Y.Q., Qu, H.L., Wu, Z.L., Zhao, X.M., 2000. Microstructure and properties of burn-resistant Ti-Al-Cu alloys. J. Mater. Sci. 35, 5609–5612.